FROM: Rotational Dynamics of Small and Macromolecules in Liquids, Lecture Notes in Physics, 293, T. Dorfmüller and R. Pecora, eds. 89-142, Springer-Verlag, 1987.

MOLECULAR ROTATIONAL DYNAMICS IN ISOTROPIC AND ORIENTED FLUIDS STUDIED BY ESR*

Jack H. Freed

Baker Laboratory of Chemistry
Cornell University
Ithaca, NY 14853 / USA

Table of Contents

*Supported by NSF Grants DMR 86-04200, CHE 83-19826, and NIH Grant GM 25862.

1. Introduction

ESR (like NMR) has for many years been utilized successfully in the study of rotational dynamics in liquids [1-4]. Our aim in this chapter is to present a reasonably up-to-date prospectus on the subject. I have chosen to do this with a variety of recent examples, largely from our laboratory, since I am most familiar with them.

Thus, in Section II, I describe the results of pressure and temperature-dependent spin-relaxation studies which led us to propose a new "quasi-hydrodynamic" model of rotational reorientation: the expanded-volume model. In Section III, ESR observations of deviations from Debye spectral densities at higher frequencies are described, and interpretations in terms of localized dynamic cooperativity are suggested. These studies are based upon the traditional measurements of T_2's or linewidths of motionally-narrowd ESR spectra. In Section IV we introduce experiments that require a more elaborate analysis than those required for the T_1 and T_2 of motionally-narrowed spectra. These are slow-motional ESR studies of rotational dynamics. They are representative of a subject I like to refer to as "Beyond T_1 and T_2", for which considerably more sophisticated analyses may be required, but more microscopic details about the motions may be forthcoming. After first illustrating the special features of rotational motions in liquid crystals in Section V, I review in Section VI our theoretical approach for analyzing slow (and fast) motional spectra in both isotropic and ordered fluids. In the first part I summarize the formulation of the theory in terms of the stochastic-Liouville equation; then I describe the powerful modern computational algorithm that we employ to solve the lineshape problem; this is followed by some of our current ideas on modeling of rotational dynamics and dynamic cooperativity.

The precise nature of the changes in molecular dynamics at a phase transition is a fascinating one, particularly at a second-order phase transition where the macroscopic equilibrium and transport properties appear to diverge. I summarize in Section VII our recent studies on spin-relaxation at the nematic to smectic A phase transition, which includes our model proposed to explain the observed critical divergences. This model emphasizes the special importance of rotational-translational couplings in highly ordered phases such as smectic phases. This suggests that a complete understanding of rotational motions requires that we also understand the translational motions in such phases. Thus, in Section VIII, I summarize our recent efforts to study the translational diffusion of ESR probes in ordered phases.

To illustrate the importance of rotational dynamics in fields other than chemical physics, I describe in Section IX our recent studies on rotational motions in model membrane systems. These are of biophysical interest, but we show how the methods and applications described in the previous Sections can be employed effectively for these more complex "ordered fluids". In particular I discuss the dynamic molecular structure and phase transitions in oriented lipid multilayers and lipid-macromolecule interactions.

Finally, In Section X, I describe new electron-spin-echo techniques that are being developed to deal more effectively with the "beyond T_1 and T_2" regime of study, and which have the promise of revolutionizing how ESR is utilized in the study of rotational motions.

II. Quasi-Hydrodynamic Models of Rotational Reorientation

In an extensive study of the pressure and temperature dependence of the electron-spin relaxation of the small nitroxide spin probe PD-Tempone in toluene solvent [5], we found significant deviations from Stokes-Einstein (SE) behavior for the rotational correlation time τ_R, where τ_R ranged over more than two orders of magnitude (cf. Fig. 1). (We shall mean by the SE relation that $\tau_R = v_e \eta / k_B T$ where v_e is an "effective molecular volume", η is the solvent viscosity and T the temperature.) These deviations were found

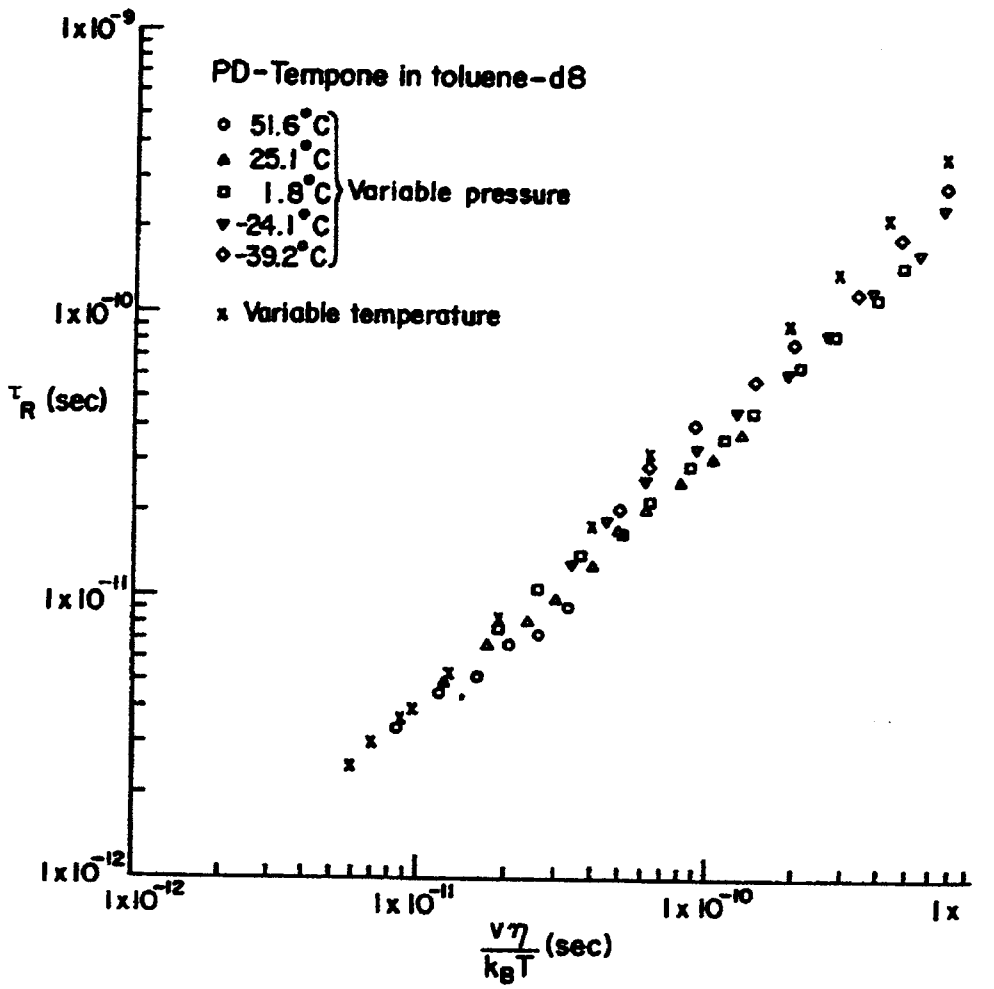

Fig. 1a: τ_R vs. $v_e \eta / k_B T$ for PD-Tempone in toluene-d8. Variable pressure and temperature results. T varied from -40°C to +50°C. P varied from 1 bar to 5.5 kbar. (From Ref. [5].)

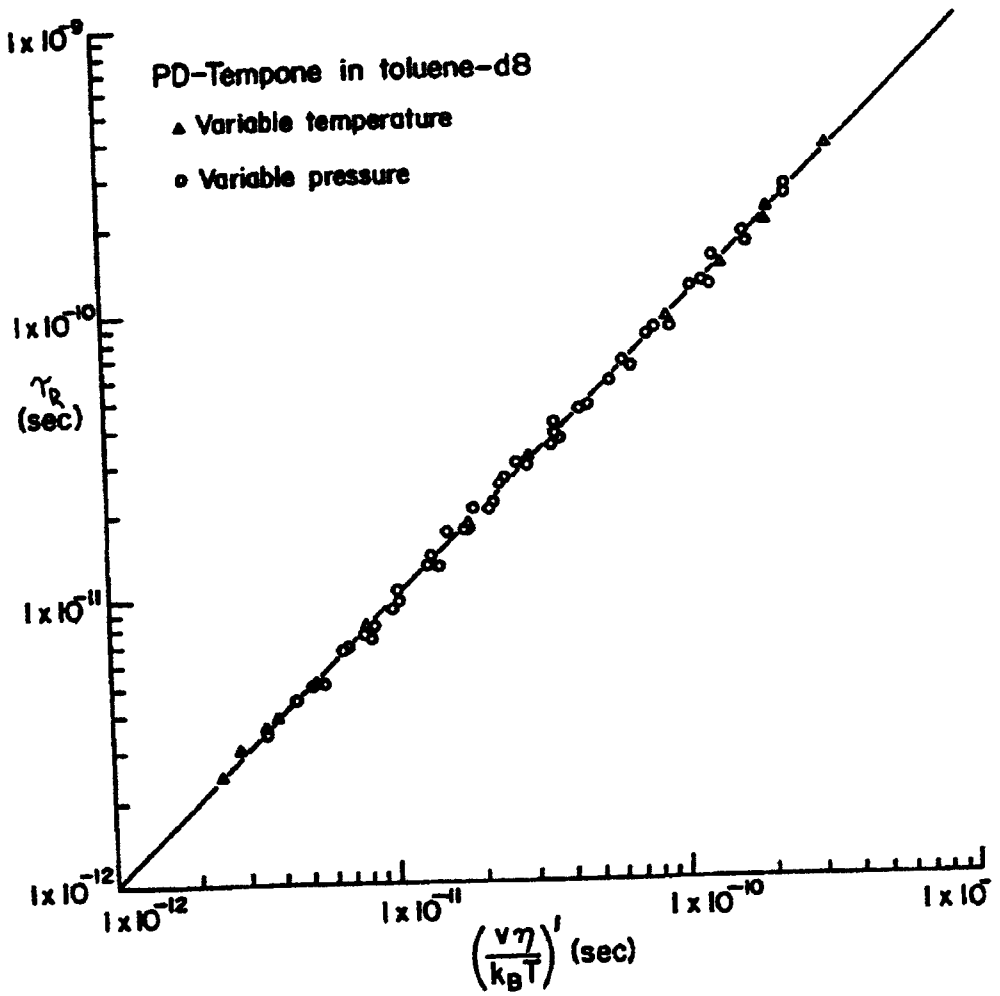

Fig. 1b: τ_R vs. $(\nu_e\eta/k_BT)'$ for PD-Tempone in toluene-d8. Variable pressure and temperature results. The identity line is included for comparison. $(\frac{\nu_e\eta}{k_BT})' = d + a_1P + a_2P^2 + b_2T^2 + cPT$ where coefficients were fit by least squares. (From Ref. 5).

to be inconsistent with hydrodynamic and molecular models previously used to interpret rotational relaxation in liquids [6-8]. These include the quasihydrodynamic free-space model of Dote et al. which has had some success in correlating a range of experimental results [7] as well as the empirical approach of Alms et al. [8] who modified the SE expression to be $\tau_R = \nu_e\eta/k_BT + \tau_R^o$ such that the data are fit to the two adjustable parameters ν_e and τ_{Ro} (cf. Table 1).

Instead, we were able to establish a simple empirical expression relating τ_R to basic hydrodynamic and thermodynamic properties [5]:

$$\tau_R = C\eta\beta_T(\rho - \tilde{\rho})/T \qquad (1)$$

where β_T is the isothermal compressibility of the solvent, and ρ is the solvent density. There are just two empirical constants: C and the reference density $\tilde{\rho}$, (= 0.819 gm/cm^3) needed to accurately fit the numerous data points obtained under a

Table I: Least-squares results for $\tau_R(T)$ vs. $\eta(T)/T$ at constant pressure. The approach of Alms et al. [9] implies that τ_R^0 should be the same and positive for all isobars (from Ref. [5]).

Pressure (kbar)	Slope (10^{-7} sK/P)[a]	Intercept (10^{-12} s)[a]
0.001	2.47 ± 0.06	-0.0 ± 0.3
0.5	2.89 ± 0.09	-1.6 ± 0.6
1	2.94 ± 0.05	-3.3 ± 0.5
1.5	2.54 ± 0.07	-2.9 ± 0.9
2	2.52 ± 0.05	-4.3 ± 0.9
2.5	2.36 ± 0.09	-4.4 ± 2.5
3	2.6 ± 0.2	-12 ± 7
3.5	2.7 ± 0.2	-21 ± 12
4	2.7 ± 0.2	-30 ± 17
4.5	2.8 ± 0.2	-49 ± 26

a) Uncertainties represent average deviations.

wide range of T and P (cf. Fig. 2). (The accuracy was as good as shown in Fig. 1b which was just an expansion in powers of P and T and required five parameters.) This empirical equation could be interpreted in terms of an "expanded volume" model. That is, $\tilde{V} = \tilde{\rho}^{-1}$ is a solvent reference volume, the "expanded volume", such that as the solvent volume $V \to \tilde{V}$ (where $V = \rho^{-1}$), then $\tau_R \to 0$. Actually this is an ideal reference state, not realized in real systems, because Eq. (1) relates to purely viscous motion, and as $V \to \tilde{V}$, the liquid is becoming more gaslike, so inertial effects would take over. Over the range of our experiments, it was demonstrated that PD-Tempone exhibits purely viscous behavior, so no inertial effects were present to complicate the viscous dynamics. The expanded volume expression takes into account in a natural way the concept of slip of the rotating molecule in the solvent, which is often introduced in an ad-hoc manner [6,7]. In another point of view we can rewrite Eq. (1) based on recognizing $\beta_T \propto c^{-2}$, where c is the sound velocity in the solvent. Then the ratio $(\tilde{V} - V)/c^2$ would appear in Eq. (1), and it is a measure of the importance of the anisotropic intermolecular interactions acting on the solute (proportional to $\tilde{V} - V$) relative to the total intermolecular interactions between molecules in the liquid (proportional to c^2). This point of view is consistent with earlier theoretical analyses of Kivelson and co-workers [10].

We believe this result is potentially important in improving our understanding of molecular rotational dynamics in liquids. Further experiments are most certainly

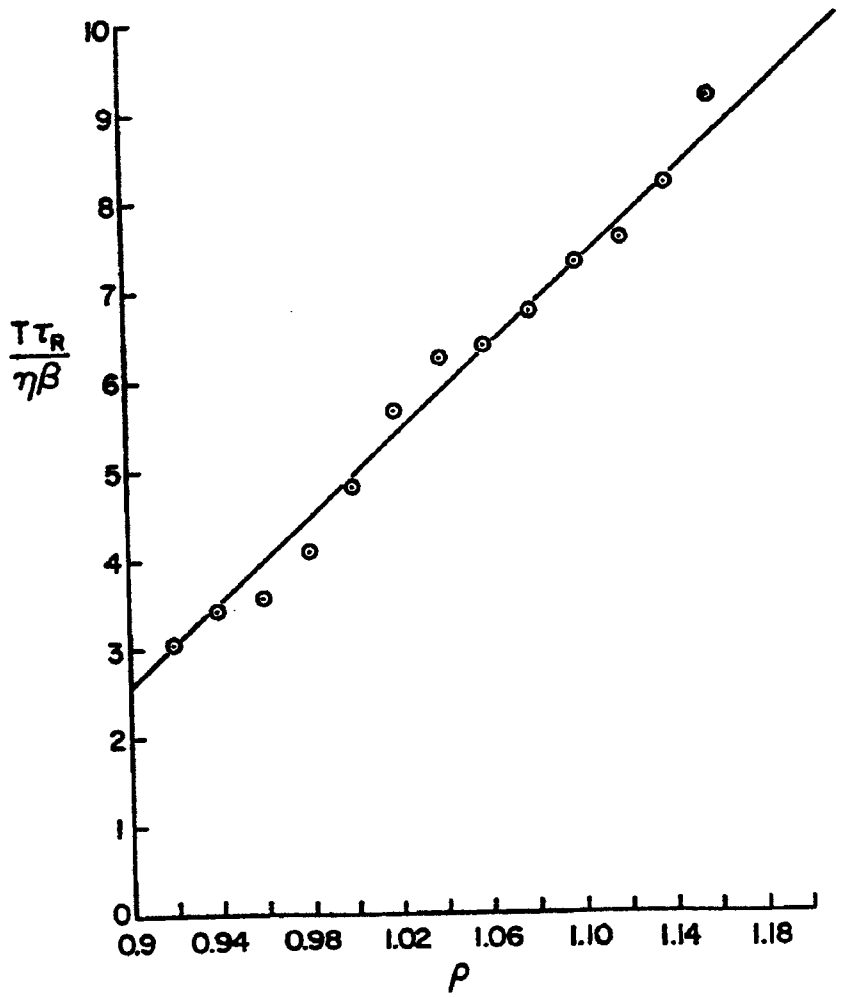

Fig. 2: Plot of average value of $\tau_R T/\eta\beta_T$ for each constant density group of data from Fig. 1 vs. density, ρ, (from Ref. [5]).

required. One should test the applicability of Eq. (1) over a wide range of solvents and solutes by means of pressure-dependent studies. Furthermore, the role of ν_p/ν_s (i.e. the ratio of probe-molecule volume to solvent-molecule volume), which should be important, needs to be studied in some detail. This ratio plays an important role in the theory of Dote et al. [7]. In our expanded volume model we expect that the reference volume $\tilde{V} = \tilde{V}(\nu_p/\nu_s)$, (i.e. it is a function of ν_p/ν_s) and that it probably also depends on the shape (i.e. deviation from sphericity) of the probe molecule. As $\nu_p/\nu_s \to \infty$, we would expect $\tilde{V}/V \to \infty$ consistent with the approach to a Stokes-Einstein limit of Eq. (1). Based upon the partial success of the theory of Dote et al. to a range of data [7], and to our success using Eq. (1) to the very precise and detailed data obtained as a function of P and T, we believe that a "quasi-hydrodynamic" model for rotational relaxation in liquids can be developed, which can fairly accurately fit a wide range of data.

When one compares our results [5] to previous pressure-dependend ESR studies of $VO(acac)_2$ (i.e. Vanadyl acac) in toluene and other solvents [11] and to NMR studies on neat liquids [12], one notes that for the former, the solvent molecules were small compared to the solute molecules, which favors Brownian rotational diffusion, while for the latter, where solvent and solute are the same, there are inertial effects. Our results of PD-Tempone in toluene probably represent an intermediate case, where the solute molecule is only a little larger than the solvent molecule, with somewhat different shape and intermolecular interaction with the solvent, and yet one is still in a regime of T and ρ where inertial effects are negligible. This regime would thus be a very favorable one for further study on molecular dynamics.

III. Non-Debye Spectral Densities

Our group has in recent years obtained extensive data on the frequency-dependence of the spectral densities due to rotational motion of probes such as PD-Tempone and

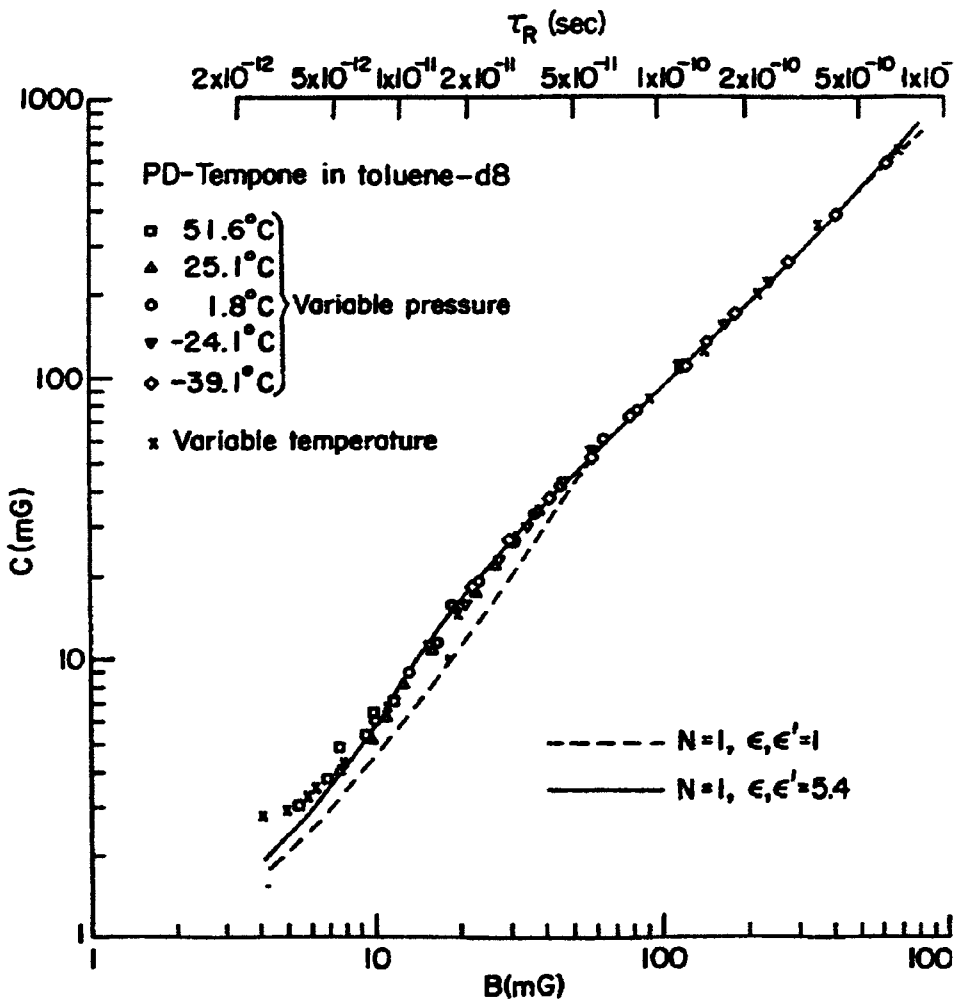

Fig. 3: A comparison of experimental and calculated values of linewidth coefficients C vs. B for PD-Tempone in toluene-d8. Variable pressure and temperature results. (From Ref. [5].)

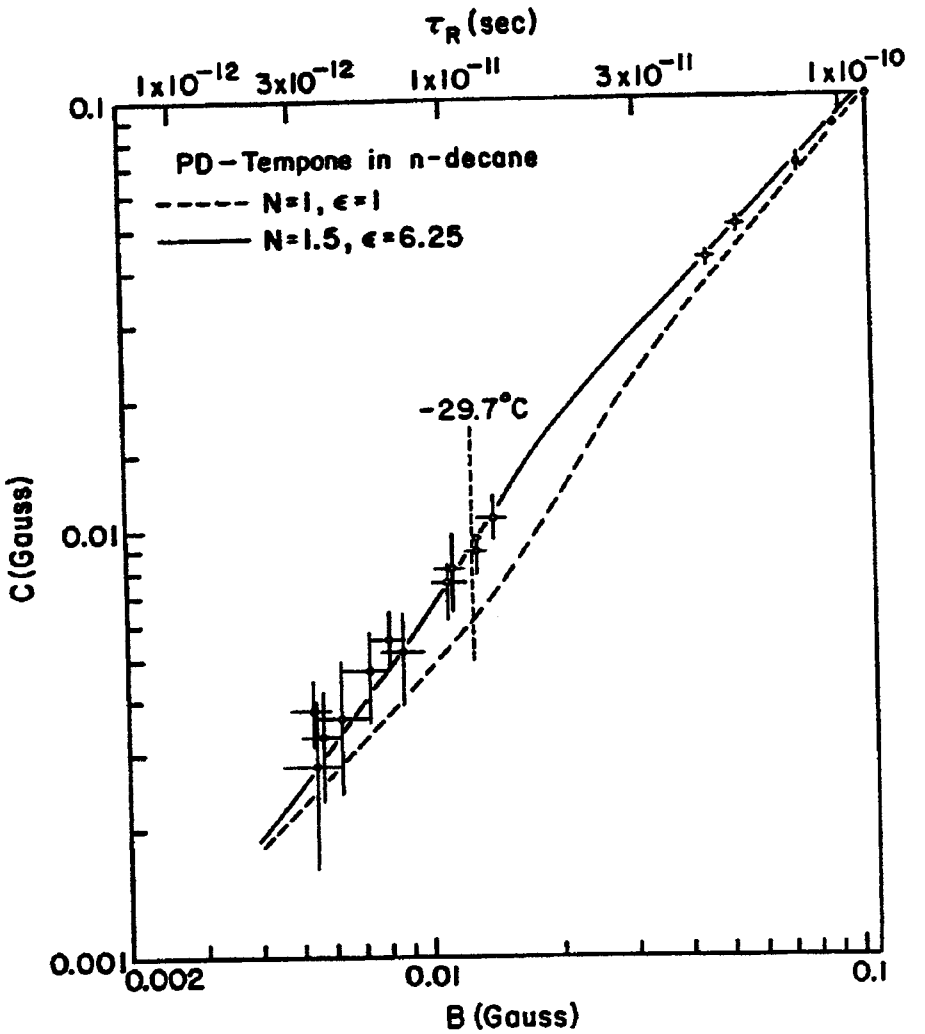

Fig. 4: Comparison of experimental and calculated values of C vs. B for PD-Tempone in n-decane. (From Ref. [13].)

peroxylamine disulfonate (PADS) [5,13-15]. We find, quite generally, that we must modify the Debye spectral density with a dimensionless factor $\varepsilon \neq 1$ (cf. Figs. 3&4):

$$j(\omega) = \frac{\tau_R}{1+\varepsilon\omega^2\tau_R^2} . \qquad (2)$$

We have interpreted this ε-correction as due to the effects of fluctuating torques acting on the probe, which relax on a time scale of the order of τ_R itself. More phenomenologically, an $\varepsilon \neq 1$ can be attributed to viscoelastic effects in the liquid. Thus, the fluctuating torque model is a particular model for "explaining" the viscoelesticity in these cases. We have found an inverse correlation between ε and solvent polarity that is consistent with this model (cf. Fig. 5) [9]. Also Patron et al [16] have reported results which show $\varepsilon > 1$ for the larger probe $VO(acac)_2$ in long chain hydrocarbons, which would be consistent with our model.

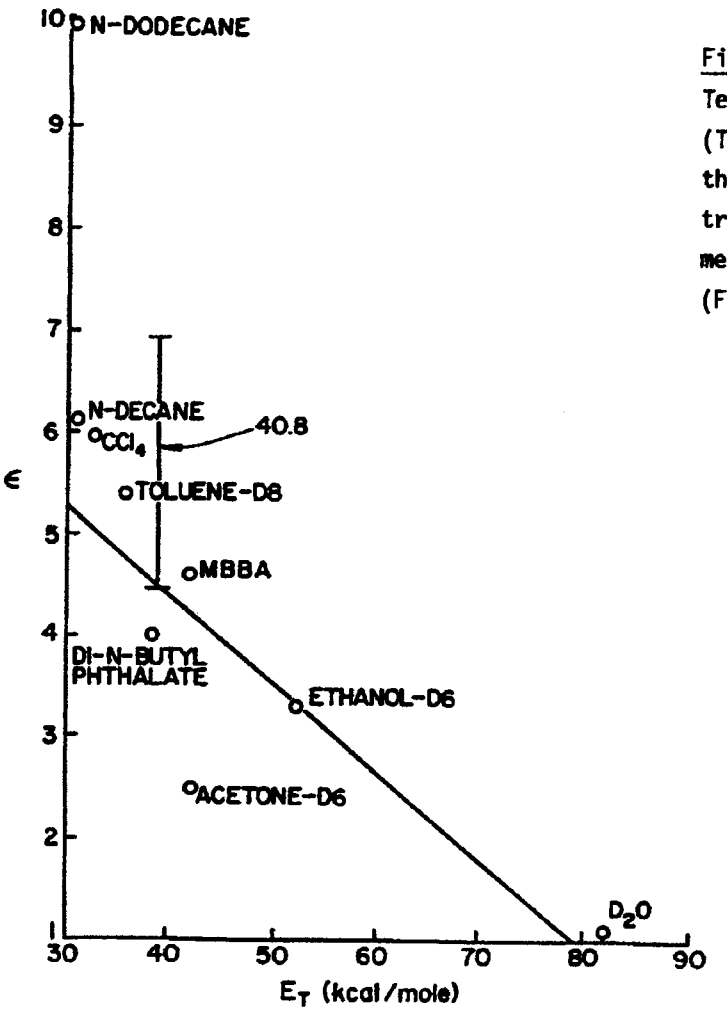

Fig. 5: ε vs. E_T for PD-Tempone in several solvents. (The line is drawn to guide the eye.) E_T, the molar transition energy, is a measure of solvent polarity. (From Ref. [13].)

One should note that it is very difficult to study the ε-correction of Eq. (2) by NMR, because the lower frequencies lead to the extreme narrowing condition for liquids. Blicharska et al. [17] have succeeded, in a study of CH_3OH in $(CD_3)_2SO$ to reach the $\omega\tau_R \propto 1$ regime. They observed definite anomalies, which we find to be consistent with an $\varepsilon > 1$.

Further work on varying probe size and solvent to distinguish between the relative importance of solvent polarity and relative solute size would be valuable, as would frequency-dependent experiments to properly study Eq. (2) and its variations.

In our attempts at interpreting Eq. (2) we have also considered another model which leads to non-Debye spectral densities [13]. It is referred to as the slowly relaxing local structure (SRLS) model, originally introduced [18] in studies on liquid-crystalline solvents. In this model, the slowly fluctuating components of the anisotropic intermolecular potential are regarded as a local structure, which presists for a mean time τ_x, and with respect to which the probe rotates, since $\tau_x > \tau_R$. Then, on this longer time scale τ_x, the local structure relaxes (or else the probe

diffuses - or jumps - away).

Our results [5,13] were generally better represented by the form of Eq. (2) with a constant ϵ than with SRLS, although our analyses could not be regarded as conclusive. Recently van der Drift and Smidt [19] working with a specially constructed cw ELDOR spectrometer obtained results that offered a systematic test to the ϵ-model of Eq. (2). They found that their data could not be fit with just a constant ϵ, but instead required a significant SRLS component even for PD-Tempone in toluene. Also, in analyzing their data, they could obtain good agreement between τ_R and τ_J (the angular-velocity correlation-function obtained from the spin-rotational relaxation terms) according to the Hubbard-Einstein relation: $\tau_R\tau_J = I/6kT$ (where I is the moment-of-inertia of the probe). The apparent breakdown of this relation in many ESR and NMR studies has been a matter of significant theoretical concern [14,20]. Further work with modern ESR techniques, such as the spin-echo methods described in Section X should be very rewarding on these matters.

IV. Slow Motional ESR Studies of Rotational Dynamics

Over a number of years we have developed highly sophisticated methods for simulating ESR (and NMR) slow motional spectra [14,15,18,21]. Such spectra are important in the study of molecular rotational dynamics by ESR in viscous media such as in liquid crystals, in spin-labeling applications in biophysics, and in polymer physics. By the slow-motion regime, we mean that the rotational motions which can average the orientation-dependent spin Hamiltonian $H(\Omega)$ (see Section VI) are too slow, i.e. we are in the regime where $\tau_R^2 \overline{H^2(\Omega)} > 1$. These spectra are no longer simple Lorentzians but are, in general, more complex in shape.

Such spectra provide considerably more information about the microscopic models of rotational dynamics than motionally narrowed spectra. Thus, for example, jump models of rotational reorientation lead to slow motional spectra which are distinguishable from Brownian reorientational models. PD-Tempone, in particular, showed deviations from Brownian rotation that appeared to be fit by a model of moderate jumps [14,15,21] (but see Section X). We have, however, suggested that a more fundamental analysis of the motional dynamics may be required as the experimental results associated with slow tumbling become more precise [14]. That is, fluctuating torques or else SRLS may be important, and the slow-motional spectra could be providing unique information on these microscopic details. VO^{2+} complexes with a vanadyl nuclear spin of $I = 7/2$ were found to be more sentitive to motional model than are nitroxides with $I = 1$ [22], (cf. Fig. 6). In particular, the slow tumbling lineshapes seem to be strongly dependent upon the nature of the ligands and of the solvent (cf. Fig. 7). Furthermore, because the vanadyl magnetic tensor components are about an order of magnitude greater than those for nitroxides, the vanadyl spectra exhibit slow motional (hence model-dependent) effects for $\tau_R > 10^{-10}$ sec. (at X-band), i.e., an order of magnitude sooner. Thus a

greater range of liquids may be studied in the slow-motional region (before they freeze) by use of vanadyl probes.

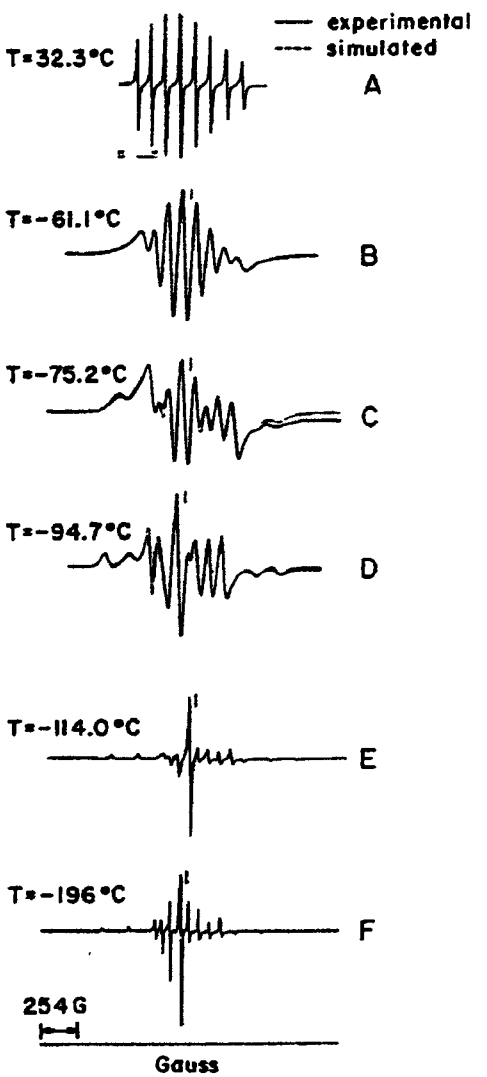

Fig. 6: Comparison of experimental and simulated spectra from the rapid motional to the rigid limit for $VO(acac_2(pn))$ in toluene. All simulations use a Brownian rotational diffusion model. (A) $\tau_R = 2.06 \times 10^{-11}$s, (B) 2.63×10^{-10}s, (C) 5.00×10^{-10}s, (D) 2.25×10^{-10}s, (E) 5.0×10^{-8}s, (F) rigid limit. (From Ref. [22].)

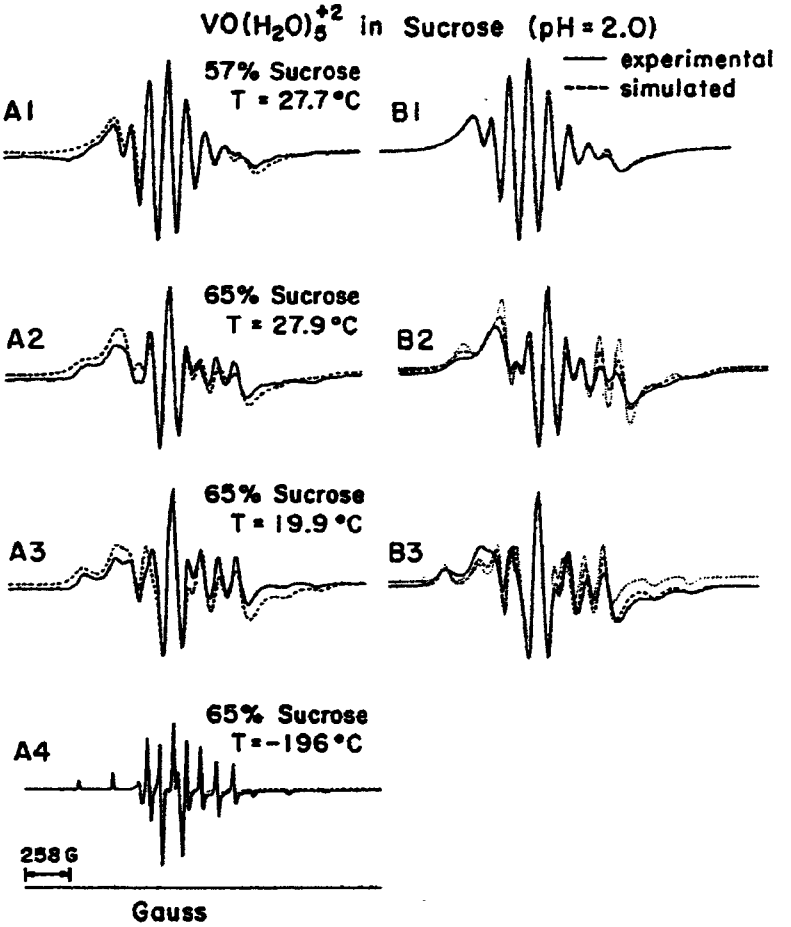

Fig. 7a: Model dependence of $VO(H_2O)_5^{2+}$ in sucrose. (Series A) Comparison of experiment with moderate jump diffusion. (Series B) Comparison of moderate jump diffusion (solid lines) with its free (dashed lines) and Brownian (dotted lines) diffusion equivalent. (Moderate jump gave best agreement in all cases.) (A1) $\tau_R^J = 3.4 \times 10^{-10}$s, (A2) 6.0×10^{-10}s, (A3) 9.0×10^{-10}s, (A4) rigid limit.

V. Liquid Crystals

The important new feature of molecular rotational dynamics in liquid crystals is that it must occur relative to a mean orienting potential. This is readily included in the theoretical analysis as described in Section VI.

In our studies on liquid-crystalline solvents we found it necessary to introduce the slowly-realxing local structure (SRLS) model in addition to the effects of the mean orienting potential [18,23,24]. In this SRLS model (as noted above) the slowly fluctuating components of the anisotropic intermolecular potential are regarded as a local structure, which persists for a mean time τ_X, and with respect to which the probe rotates, since $\tau_X \gg \tau_R$. Then, on this longer time-scale τ_X, the local structure relaxes (or else the probe diffuses or jumps away). This seems a reasonable model for

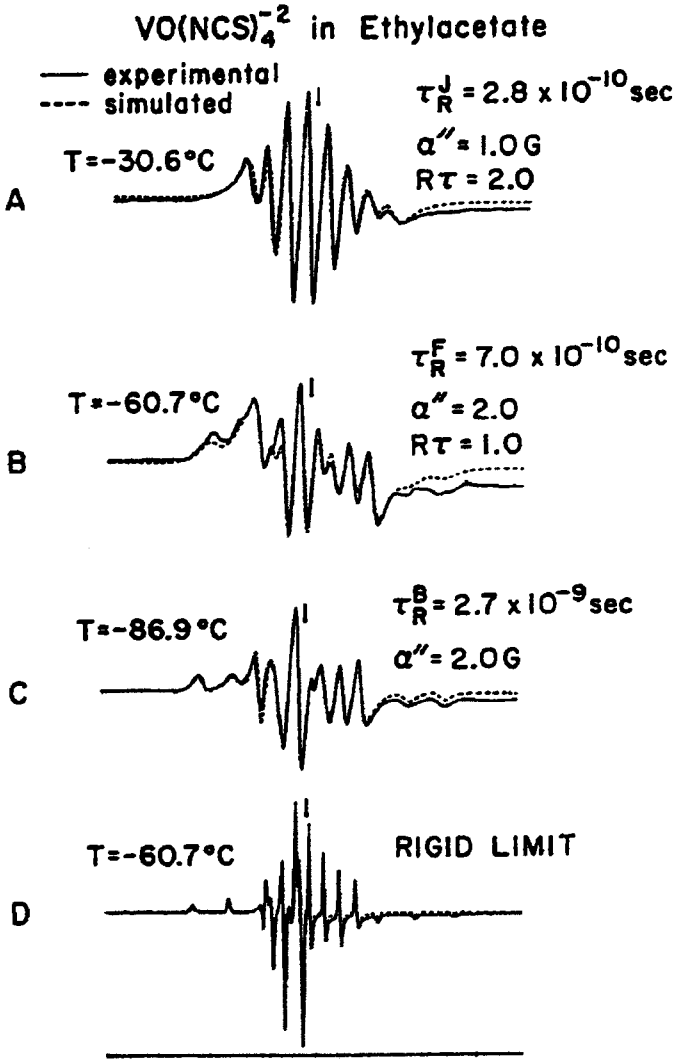

Fig. 7b: Model dependence of $VO(NCS)_4^{2-}$ in ethyl acetate. Note that A is approximately fit with moderate jump, B with free diffusion, and C with Brownian diffusion. (From Ref. [22].)

probes that are smaller than the liquid crystalline molecules, since they reorient in times much shorter than the surrounding solvent molecules. Again the evidence comes from our detailed linewidth studies of smaller probes such as PD-Tempone [18,23,24]. In particular, in a pressure-dependent study of PD-Tempone in the nematic Phase V solvent, we concluded that the SRLS contribution to the linewidths might be comparable to the normal reorientational contribution from which τ_R is estimated [23]. Thus, τ_R's calculated from $j(\omega)$ might be significantly larger than the true value, but the data just from the linewidth coefficients are insufficient to be definitive on this latter point. In our studies of smectics we find even more substantial linewidth anomalies attributable to the SRLS model [24]. This is reasonable in the context of

our model (discussed below) for the smaller probe in the smectic phases; viz. these probes are now located in the more flexible alkyl-chain regions, experiencing the slow (cooperative) fluctuations of these chains.

Acronym	Name	Structure
PD-Tempone	2,2', 6,6'-tetramethyl-4-piperidine N-oxyde (perdeuterated)	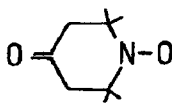
P	2,2', 6,6'-tetramethyl-4-(butyloxyl)-benzylamino-piperidine 1-oxyl (perdeuterated piperidine ring)	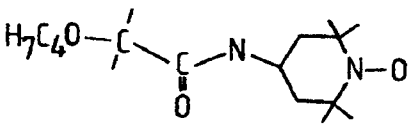
MOTA	4-methylamino 2,2', 6,6'-tetra-methyl-piperidine-1-oxyl (perdeuterated ring)	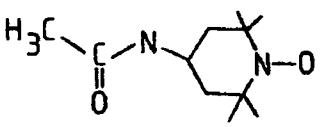
CSL	3,3'-dimethylorazolidinyl-N-oxy 2'3-5a-cholestane	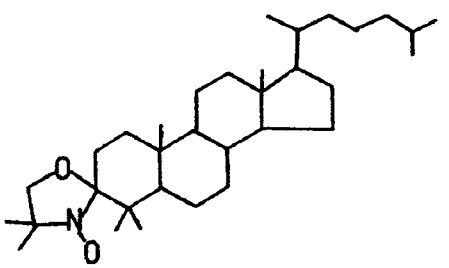

Fig. 8: Structures of spin probes in our studies.

We show in Figs. 8 and 9 some spin probes used in our studies and some liquid crystals we have used. In Fig. 10 we illustrate how ESR lineshapes are sensitive to both the orienting potential and the rotational dynamics relative to this potential for the P-probe, which is comparable in size and shape to a liquid crystal molecule [25]. The variations in ordering and rotational rates for the isotropic, nematic, smectic A and smectic B phases are illustrated in Fig. 11. This probe experiences an orienting alignment similar to that of liquid crystalline molecules (except that there is some flexibility for internal rotational motion of the nitroxide moiety). Shown in the inset to Fig. 11 is the related data [24] for the small PD-Tempone probe. The unusual observation here is the very low activation energy for rotation of this probe in the two smectic phases even though it is substantially higher in the isotropic and nematic phases. This is taken as significant evidence to support the model [24] that this probe

Acronym	Name	Formula
6OCB	4-cyano 4'-n-hexyloxybiphenyl	NC-ϕ-ϕ-OC_6H_{13}
8OCB	4-cyano 4'-n-octyloxybiphenyl	NC-ϕ-ϕ-OC_8H_{17}
40,6	N-(p-butoxybenzylidene)-p-n-hexylaniline	H_9C_4O-ϕ-CHN-ϕ-C_9H_{13}
40,8	N-(p-butoxybenzylidene)-p-n-octylaniline	H_9C_4O-ϕ-CHN-ϕ-C_8H_{17}
8CB	4-cyano 4'-n-octylbiphenyl	NC-ϕ-ϕ-C_8H_{17}
S2	Eutectic mixture of: 50% 4-cyano 4'-n-octylbiphenyl 39% 4-cyano 4'-n-decylbiphenyl 11% 4-cyano 4'-n-decyloxybiphenyl	 NC-ϕ-ϕ-C_8H_{17} Nc-ϕ-ϕ-$C_{10}H_{21}$ NC-ϕ-ϕ-$OC_{10}H_{21}$

Transition Temperatures of some Liquid Crystals:

a. 27% 6OCB - 73% 8OCB : K (24^o) N (31^o) S_A (45^o) N (79^o) I

b. 40,6 : K (18^o) S_B (48^o) S_A (55^o) N (78^o) I

c. 8CB : K (21^o) S_A (34^o) N (41^o)

d. S2 : K (-10^o) S_A (48^o) N (49^o) I

Fig. 9: Some liquid crystals used in our studies.

is expelled into the chain region of the smectic layers, since it is known that the activation energy for reorientation for PD-Tempone in neat aliphatic hydrocarbons is just 2-4 kcals [13].

Additional strong evidence for this "expulsion effect" in the smectic phases is shown in Figs. 12 and 13. In Fig. 12 we show the ordering of PD-Tempone (in 40,8) in the different phases [24]. In the S_A phase this probe experiences a reduction in its ordering as the temperature decreases which is contrary to the increasing ordering of the liquid crystal molecules (cf. Fig. 11). This is readily interpreted as due to the probe being increasingly expelled into the less ordered aliphatic chain region. In Fig. 13 we show a plot of the PD-Tempone hf splitting for different solvents arranged according to their relative polarity [24]. Aliphatic hydrocarbons, being the most non-planar, yield the lowest hf splitting. Indeed PD-Tempone in 40,6 and 40,8 shows a decrease in its hf splitting as the temperature is lowered into the smectic phases in a manner consistent with its being dissolved more into the aliphatic hydrocarbon region.

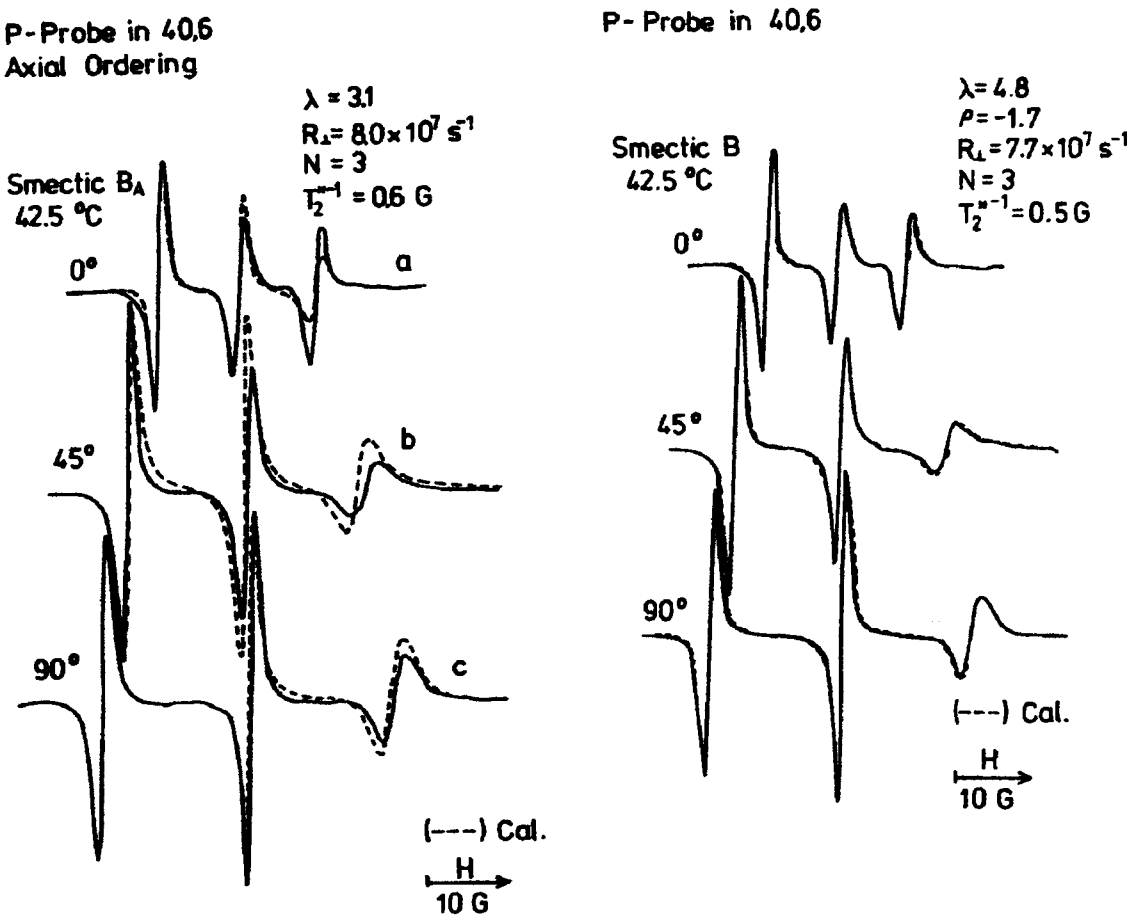

Fig. 10: (___) Experimental and (---) calculated ESR spectra of P probe dissolved in 40,6 oriented between plates and in the smectic B_A phase of 42.5°C. The angle θ between the magnetic field B and the plate normal is denoted in the Figures. The ordering parameters and rotational rates (given by $R_\perp$, the perpendicular component of the rotational diffusion tensor, and $N = R_\parallel/R_\perp$ the rotational asymmetry) are on the figures. (a) corresponds to cylindrically symmetric ordering given by $\lambda(5/4\pi)^{1/2} = \epsilon_0^2/kT$, while in (b) an asymmetry term of $\rho(5/4\pi)^{1/2} = \epsilon_2^2/kT$ [cf. Eq. (7)] is allowed. (From Ref. [25].)

VI. Theoretical Approach

A) Stochastic Liouville Equation

The basis for our analysis in the above studies is the stochastic Liouville equation (SLE). One starts with the spin density-matrix equation of motion for ρ:

$$\frac{\partial \rho(t)}{\partial t} = -i\,[H(t), \rho] \qquad (3)$$

where $H(t)$ is the time-varying spin-Hamiltonian due to fluctuations of Euler angles Ω of the molecule with respect to the lab frame. A classical stationary Markovian

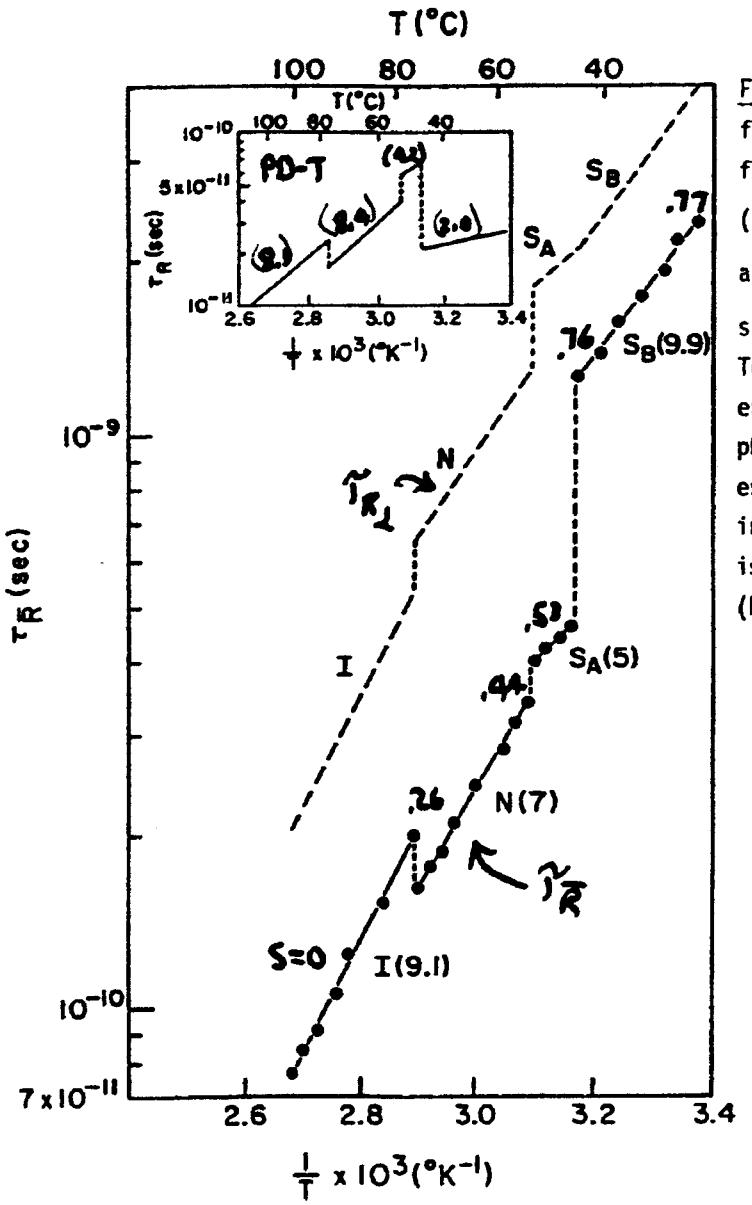

Fig. 11: Rotational rates for $\tau_{\bar{R}}$ and $\tau_{R_\perp}$ vs. 1/T for the P-probe in 40,6. (Here $\tau_{\bar{R}} \equiv 6^{-1}(R_{||}R_\perp)^{-1/2}$ and $\tau_{R_\perp} = 6_\perp^{-1}R^{-1}$). Insert shows τ_R vs. 1/T for PD-Tempone in 40,6. Activation energies in the respective phases are shown in parenthesis, and the range of ordering for P-probe in each phase is also given. (From Ref. [25].)

description for the orientational probability distribution $P(\Omega,t)$ is assumed. That is we let

$$\frac{\partial P(\Omega,t)}{\partial t} = -\Gamma_\Omega P(\Omega,t) \tag{4}$$

where Γ_Ω is the time-independent "diffusion" operator. Then one can show that the composite set of spin and space variables obeys the SLE:

$$\frac{\partial \rho(\Omega,t)}{\partial t} = -i([H(\Omega),\rho] - \Gamma_\Omega \rho(\Omega,t) \tag{5}$$

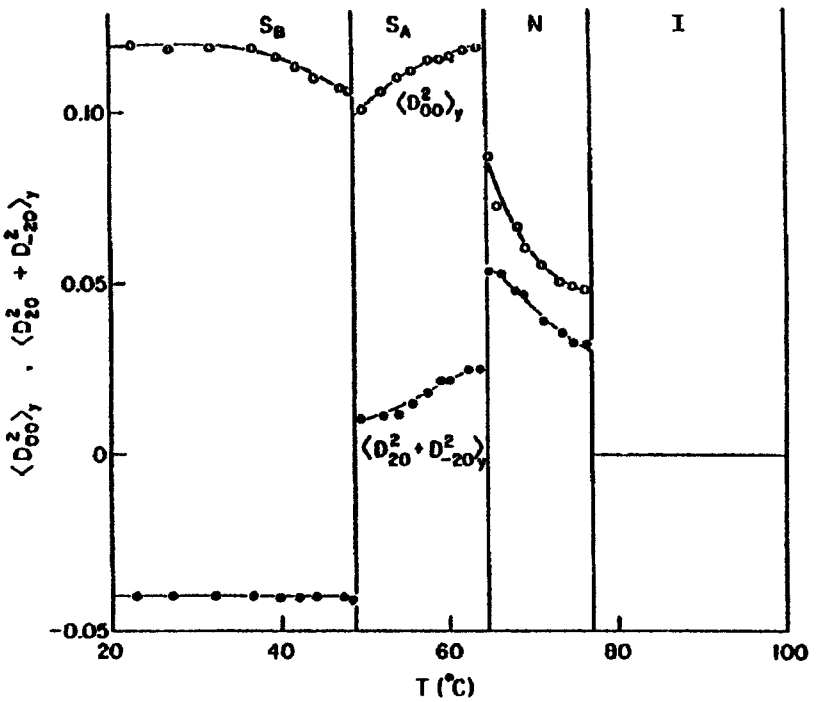

Fig. 12: Order parameters for PD-Tempone in 40,8. Here $\langle D^2_{00}\rangle = (5/4\pi)^{1/2}\langle Y^2_0\rangle$ and and $\langle D^2_{00} + D^2_{0-2}\rangle = (5/4\pi)^{1/2}\langle Y^2_2 + Y^2_{-2}\rangle$. The break in ordering parameters at N-S_A transition is an experimental artifact. (From Ref. [24].)

where now $\rho(\Omega,t)$ is simultaneously the quantum-mechanical spin-density matrix and the classical probability distribution function in molecular orientation. To simplify the analysis one typically chooses [18,21,28] a Smoluchowski equation for Γ_Ω:

$$\Gamma_\Omega = -\underset{\sim}{M}\cdot\left[\left(\underset{\approx}{R}\, M\, \frac{U(\Omega)}{kT}\right) + \underset{\approx}{R}\cdot\underset{\sim}{M}\right]. \qquad (6)$$

Here $\underset{\sim}{M}$ is the vector space for infinitesimal rotation, $\underset{\approx}{R}$ is the rotational diffusion tensor, and $U(\Omega)$ is the equilibrium potential for the orientation of the probe, which may be expanded in spherical Harmonics, $Y^L_K(\Omega)$ according to:

$$U(\Omega) = \sum_{\substack{\text{even}\\ L}}^{\infty}\left\{\varepsilon^L_0\, Y^L_0(\Omega) + \sum_{K>0}^{L}\varepsilon^L_{K\pm}\left[Y^L_K(\Omega) \pm Y^L_{-K}(\Omega)\right]\right\}. \qquad (7)$$

Typically only the $L = 2$ terms are kept (but sometimes terms through $L = 4$ are included [29], cf. Fig. 14). One can even allow for dynamic cooperativity by letting

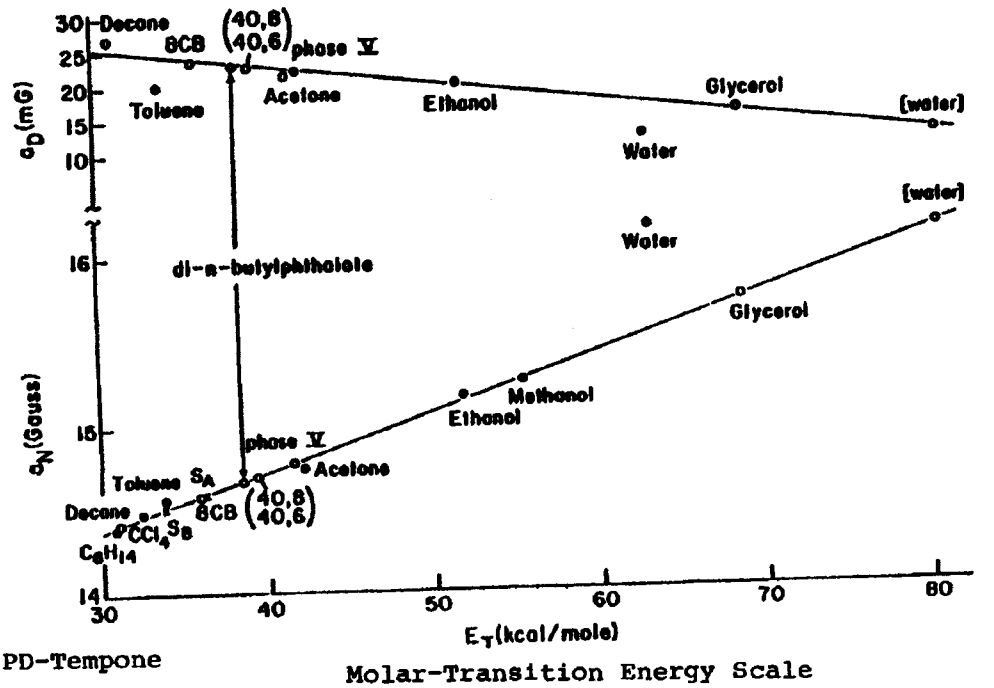

Fig. 13: Variation of hf splittings a_N and a_D for PD-Tempone with E_T (the molar transition energy) in different solvents. (From Ref. [24].)

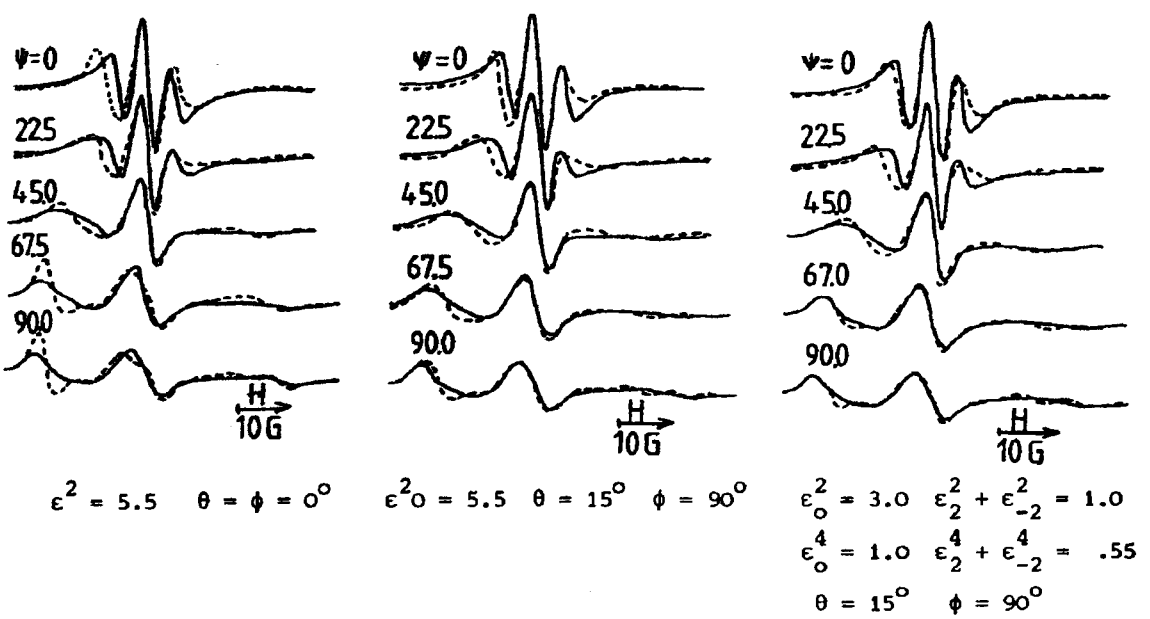

Fig. 14: Experimental spectra of homeotropically aligned CSL in S2 at -8°C for tilt angle ψ between the liquid crystal director and the external magnetic field H_0 (solid lines). Dashed lines denote simulated spectra with anisotropic diffusion in a high ordering potential. $(0,\theta,\phi)$ denote Euler angles between the magnetic frame and the ordering frame. The ε^L_K denote coefficients in the expansion of the ordering potential in spherical harmonics. (From Ref. [29].)

$U(\Omega) \rightarrow U(t)$ such that the probe reorients in the instantaneous potential field of its surroundings. This approach is used for SRLS and for coupling to hydrodynamic and critical modes [30,31]. In smectic phases the orientational potential felt by a molecular probe should depend upon the probe location within the smectic bilayer in order to be consistent with the observation of reduced ordering for some probes as they are expelled into the alkyl chain region. (Related NMR observations have also been made [32-34]). Other evidence exists that translational diffusion perpendicular to the smectic layers is highly hindered in the smectic phase [33]. Thus the probe will experience a coupled orientation-position potential as it diffuses in the spatially non-uniform smectic. Moro and Nordio have studied this [35] using as their combined potential:

$$U/kT = \{A + B\cos(2\pi z/d)\}\, Y_0^2(\beta) + C\cos(2\pi z/d) \qquad (8)$$

which is of the form utilized by McMillan [36] in his mean-field theory of the smectic phase transition. (Here β is the angle of orientation between the nematic director and the principal axis of ordering of the probe, while z measures the position in a smectic layer of thickness d). They consider small probes of dimension $d_0 \ll d$, so that they undergo many reorientations in the time they translate across a smectic layer. This model then has all the ingredients of a SRLS model. Indeed their detailed calculations showed that "the relaxation mechanism due to this order modulation is similar to those often referred to as 'slowly relaxing local structures'... " [18].

In summary, the fundamental problem in slow-motional ESR spectroscopy is to compare solutions of the SLE (Eq. (5)) with experimental spectra so as to extract out the correct stochastic operator Γ and obtain the magnitude of the relevant physical parameters. We may refer to this as solving for the "inverse stochastic Liouville Transform" (by analogy with the "inverse scattering transform" in the quantum mechanical theory of scattering). In practice this is not possible, so one constructs simple models for Γ_Ω as illustrated above, and then one calculates predicted spectra to compare with experiment as illustrated (cf. Figs. 6, 7, 10, 11).

B. Computational Algorithm

It follows from Eq. (5) that in the linear response regime, the absorption intensity $I(\Delta\omega)$ is given by [21,26,27]:

$$I(\Delta\omega) = \frac{1}{\pi} \mathrm{Re} \langle v | [i(\Delta\omega \underline{1} - \underline{L}) + \underline{\Gamma}]^{-1} | v \rangle \qquad (9)$$

where $\Delta\omega$ is "the sweep variable", $\underline{L}$ is the Liouville operator associated with the spin Hamiltonian $H(\Omega)$ of the spin probe, and $\underline{\Gamma}$ is the diffusion operator for the reorientation that modulates the magnetic interactions. Also $|v\rangle$ is the so-called "starting vector" constructed from the spin transition moment averaged over the equilibrium ensemble. The vectors and operators are defined in the direct product space

of the ESR transitions and of the functions of the Euler angles Ω. (In ESR we usually have $\Delta\omega = \omega - \omega_0$ where ω_0 is the Larmour frequency at the center of the spectrum and ω is the angular frequency of the applied radiation field.) We may rewrite Eq. (9) as:

$$I(\Delta\omega) = \frac{1}{\pi} \text{Re} \langle v|u(\Delta\omega)\rangle \tag{10}$$

where $|u(\Delta\omega)$ is the solution of the equation

$$\underset{\sim}{A}'|u\rangle = |v\rangle \tag{11}$$

the matrix $\underset{\sim}{A}'$ is defined as $\underset{\sim}{A}' = i\Delta\omega\, \underset{\sim}{1} + \underset{\sim}{A}$ where $\underset{\sim}{A} = \underset{\sim}{\Gamma} - i\, \underset{\sim}{L}$. Eq. (9) can be solved either by inversion of $\underset{\sim}{A}'(\Delta\omega)$ for a range of values of $\Delta\omega$, or alternatively by diagonalizing $\underset{\sim}{A}$ only once [21].

The matrix $\underset{\sim}{A}$ is in general very large and sparse. The conventional methods [21] for solving Eq. (11) by inversion or by diagonalizing $\underset{\sim}{A}$ prove to be too cumbersome. One soon runs out of memory even on mainframe computers, and the solution requires prohibitive amounts of computer time. To remedy this situation the Lanczos algorithm has been developed for complex-symmetric matrices, since $\underset{\sim}{A}$ is typically of this form [37,38]. It is an efficient method for tri-diagonalizing $\underset{\sim}{A}$ and is particularly suited to the solution of large-sparse matrices. We have shown that it can lead to <u>at least</u> order of magnitude reductions in computation time, and it yields solutions of Eq. (9) to a high degree of accuracy [37,39]. This Lanczos algorithm is also appropriate for the general class of Fokker-Planck equations (including models of rotational motion) which can be represented by a complex symmetric Fokker-Planck operator $\underset{\sim}{A}$ (after symmetrization). For such cases, Eq. (9) would be associated with the spectral density , which is the Fourier transform of the time correlation function of a dynamical variable $v(t)$ [37,38]. In fact, more generally, it is possible to establish the close connection between the Lanczos algorithm based upon a scheme of projection operators in Hilbert space, and the Mori projection scheme in statistical mechanics [38,40].

The LA tri-diagonalization proceeds by recursive steps or projections. If we let N be the dimension of the matrix, and n_s, the number of recursive steps needed to converge to an accurate spectrum, then we find $n_s << N$. This inequality becomes more dramatic the more complicated the problem. In this sense, the Lanczos projections rapidly seek out, from an initial finite subspace of dimension N, a smaller subspace spanned by the Lanczos vectors. That is the LA constructs subspaces that progressively approximate the "optimal reduced space" for the problem. These subspaces, spanned by the Lanczos vectors are related to Krylov subspaces [41,42] and are generated from the sequence $\underset{\sim}{A}^{k-1}|v\rangle$ for $k = 1,\ldots,n$. Thus, the choice of $|v\rangle$ as the "starting vector" biases the projections in favor of this "optimal reduced space". It is easy to

show that this Krylov sub-space can only contain eigenvectors of $\underset{\sim}{A}$ with a non-zero component along $|v\rangle$. In general, the time required for the LA tri-diagonalization goes approximately as $n_s N(2n_E + 21)$, where n_E is the average number of non-zero matrix elements in a row of $\underset{\sim}{A}$ [37].

Very recently [43] we have learned how to blend the LA with the conjugate gradient method to "turbo-charge" the Lanczos Algorithm. This more powerful version supplies objective criteria for truncation of basis sets and recursive steps.

We briefly summarize the Lanczos algorithm. We first identify the starting vector $|v\rangle$ as the first Lanczos vector $|\Phi_1\rangle$. Then a Schmidt orthogonalization on the Krylov sequence $\underset{\sim}{A}^{k-1}|v\rangle$ for $k = 1,\ldots,n$ allows one to iteratively generate the set of orthonormal Lanczos vectors $|\Phi_k\rangle$ according to

$$\beta_{k+1}|\Phi_{k+1}\rangle = (1-P_k)\,\underset{\sim}{A}|\Phi_k\rangle \tag{12}$$

where β_{k+1} is the normalizing coefficient such that

$$\langle\Phi_{k+1}|\Phi_{k+1}\rangle = 1 \tag{13}$$

and $\underset{\sim}{P}_k$ is the projection operator on the Krylov subspace spanned by $|\Phi_j\rangle$ $j = 1,\ldots,n$ given by:

$$P_k = \sum_{j=1}^{k} |\Phi_j\rangle\langle\Phi_j| \quad . \tag{14}$$

Eq. (11) leads to a three-term recursive relation for generating the $|\Phi_j$:

$$\beta_{k+1}|\Phi_{k+1}\rangle = (A-\alpha_k)|\Phi_k\rangle - \beta_k|\Phi_{k-1}\rangle \tag{15}$$

where

$$\alpha_k = \langle\Phi_k|\underset{\sim}{A}|\Phi_k\rangle \tag{16}$$

and

$$\beta_k = \langle\Phi_k|\underset{\sim}{A}|\Phi_{k-1}\rangle \quad . \tag{17}$$

It may easily be shown that $\underset{\sim}{A}$ has a tridiagonal representation, $\underset{\sim}{T}_n$ in the basis of Lanczos vectors $|\Phi_j\rangle$ such that

$$\langle\Phi_k|\underset{\sim}{A}|\Phi_j = 0 \quad \text{if} \quad k \neq j, \; j \mp 1 \tag{18}$$

while Eqs. (16) and (17) give the non-zero matrix elements. That is, given the vectors $|\Phi_k\rangle$ in terms of their components $x_{j,k}$ in the original basis set, $|f_j\rangle$, $j = 1,\ldots,N$

$$|\Phi_k\rangle = \sum_j x_{j,k} |f_j\rangle \tag{19a}$$

$$x_{j,k} = \langle f_j | \Phi_k \rangle \tag{19b}$$

then the column vectors $\underset{\sim}{x}_k$ form the orthogonal matrix $\underset{\sim}{Q}_n$ such that $\underset{\sim}{Q}_n^{tr} \underset{\sim}{Q}_n = \underset{\sim}{1}_n$ and

$$\underset{\sim}{T}_n = \underset{\sim}{Q}_n^{tr} \underset{\sim}{A}_N \underset{\sim}{Q}_n \ . \tag{20}$$

We have described the conventional Lanczos algorithm for real symmetric (or Hermitian) matrixes $\underset{\sim}{A}$ such that Eq. (13) involves the usual norms in Hilbert space.

For our present applications to ESR (and Fokker-Planck equations) for which $\underset{\sim}{A}$ is complex symmetric (or else can be transformed to complex symmetric form [37,38,40]) Moro and Freed [37,38] showed that one must introduce the Euclidean pseudo-norm. That is, first consider the general non-Hermitian case. One must introduce a biorthonormal set of functions Φ_j and $\Phi^{j'}$ such that

$$\langle \Phi^{j'} | \Phi_j \rangle = \delta_{j,j'} \tag{21}$$

or alternatively (letting $\underset{\sim}{x}^{j'}$ and $\underset{\sim}{x}_j$ be their column vector representations):

$$\underset{\sim}{x}^{j'} \cdot \underset{\sim}{x}_j = \delta_{j,j'} \ . \tag{22}$$

However, for the case of (non-defective [42]) complex symmetric matrices $\underset{\sim}{A}$, it is possible to let

$$\underset{\sim}{x}^j = \underset{\sim}{x}_j^* \tag{23}$$

such that Eq. (22) becomes:

$$\underset{\sim}{x}_j^{tr} \cdot \underset{\sim}{x}_j = \delta_{j,j'} \tag{24}$$

and then the recursion method of Eqs. (12) - (18) remains applicable with Eq. (24) defining the Euclidean pseudo-norm, whereby the bra vectors are defined without the usual complex conjugation in a Hilbert space.

Finally we note that the complex symmetric tridiagonal matrix $\underset{\sim}{T}_n$ can easily be diagonalized by one of several methods [42,44]. This is not necessary for cw-ESR spectra (or for simple spectral densities from Fokker-Planck equations), since one can use a continued-fraction solution, but it is needed for 2D-ESE spectra (cf. Sect. X).

The computational algorithms for simulating magnetic resonance spectra in terms of molecular dynamics as well as for spectral densities for molecular dynamics have recently been reviewed [83].

C. Modeling of Rotational Dynamics

In recent years [45] we have developed a useful method of stochastic modeling, which has been summarized elsewhere [46]. It is a generalization of the stochastic-Liouville method whereby the basic physics of the "relevant" degrees of freedom and their couplings may be introduced in a transparent manner, in conjunction with the stochastic features of the bath variables. The resulting incomplete stochastic Liouville equation is then subjected to the constraints required for detailed balance in order to correctly include the "back-reaction" of the bath on the "relevant" degrees of freedom. The resulting augmented stochastic Liouville equation may then be efficiently solved by the Lanczos algorithm. By means of this approach one can develop expressions for fluctuating torque, SRLS, and related models. Partially based on such ideas, we have developed soluble models for coupled reorientation of rod-like liquid crystal molecules in order to improve on the hydrodynamic model used for describing spin relaxation by director fluctuations [47]. Also, we have developed an approach. the dynamic cluster model (DCM), to incorporate the dynamic localized cooperativity in the rotational relaxation of liquid crystal molecules in nematics.

D. Modeling of Dynamic Cooperativity

Our past ESR analyses in terms of local cooperativity were based upon the slowly relaxing local structure (SRLS) model, which has now been improved by using our augmented Fokker-Planck approach. But in the highly ordered phases typical of liquid crystals, the cooperativity in reorientation may well be too great to be modeled in such a simple fashion. With the recent theoretical and computational advances, it could be feasible to analyze more realistic models of cooperative dynamics for the longer time scales (i.e. $>>10^{-12}$ sec) that are important for our magnetic resonance studies [48]. In this sense, such methods could be a useful alternative to full molecular dynamics calculations [49,50]. The particular model we have been studying is a "dynamic cluster model" (DCM) [48]. There have already been treatments of the role of short range order on the equilibrium properties of liquid crystalline phases using various forms of Bethe's cluster method [51]. In this method a central molecule is surrounded by γ nearest neighbors which form the outer shell. The central molecule interacts with this cluster through pairwise potentials $U(\Omega_0,\Omega_i)$ $i = 1,2,\ldots,\gamma$, with the Ω_i being the Euler angles for the i-th molecule. While the γ-neighbors do not interact with each other, they all feel an orienting potential $V(\Omega_i)$ representing the mean potential of the fluid. Then a self-consistency relation is introduced so that the central molecule orders exactly in the same way as do the outer shell molecules. This leads to non-trivial integral equations for solving for $V(\Omega_i)$. Ypma and Vertogen [51] obtain best results for this model for $\gamma = 3$ or 4.

The DCM we have been studying is just the dynamical version of this. We model the $\gamma+1$ particle system by the appropriate set of coupled Smoluchowski equations

for the joint probability distribution $P(\Omega_0 \ldots \Omega_\gamma, t)$. These coupled Smoluchowski equations are then solved for correlation functions such as

$$\langle Y_0^2[\Omega_0(t)] Y_0^2[\Omega_0(0)] \rangle - \langle Y_0^2[\Omega_0(0)] \rangle^2$$

by means of the Lanczos algorthim. If we regard the central molecule as a probe, then in a sense, it is not necessary to achieve self-consistency. However, the matter of self-consistency is conveniently dealt with by solving numerically the Ypma-Vertogen integro-differential equations. These equations then give us the self-consistent values of $V(\Omega_i)$ for a given value of $U(\Omega_0, \Omega_i)$. In our solution of the several-body diffusion equation $\partial P/\partial t = \Gamma P$, (actually we solve the symmetrized form), we use the analogy to the problem of the quantum mechanics of a many-electron atom. Let us call the operator Γ for the dynamic cluster problem $\Gamma_{cluster}$, while the standard problem of the diffusion of a single particle in the mean-field of its surrounding is represented by the operator Γ_{MF} (and is typically given in the form of Eq. (6)). We first solve the conventional mean field problem for $P^1(\Omega_1, t)$ in the usual manner (i.e. Eq. (4)) to yield the one-particle mean-field eigenvalues and eigenvectors appropriate for a given meanfield potential. Then we select the mean-field solution corresponding to order parameter $S = \langle Y_0^2 \rangle$ which is (nearly) equal to that for the cluster problem to be solved. That is, we regard these Γ_{MF} as the diffusional analogue of (Hartree) SCF theory, i.e. an approximation to the best one-particle solution. Then we solve for $\Gamma_{cluster}$ by methods analogous to configuration-interaction starting with these one-particle solutions of Γ_{MF}. That is, the basis states are products of the one-particle states from Γ_{MF}, and we then diagonalize Γ in this basis. The problem with this method, as in any configuration interaction, is whether we have chosen enough excited "configurations" for the calculation to converge.

Utilizing approximate basis sets (suitable for computation on a PDP11 mini-computer), we have obtained initial results for the correlation function for $Y_0^2(\Omega_1)$, and we have compared them to the mean-field results as illustrated in Fig. 15. Interestingly enough, we find that for the nematic phase, the results for the full DCM lie rather close in shape to those for the simple MF problem. However, this is not so for the isotropic phase, especially for the phase transition region for $\gamma = 3$ or 4 (where γ is the number of cluster particles).

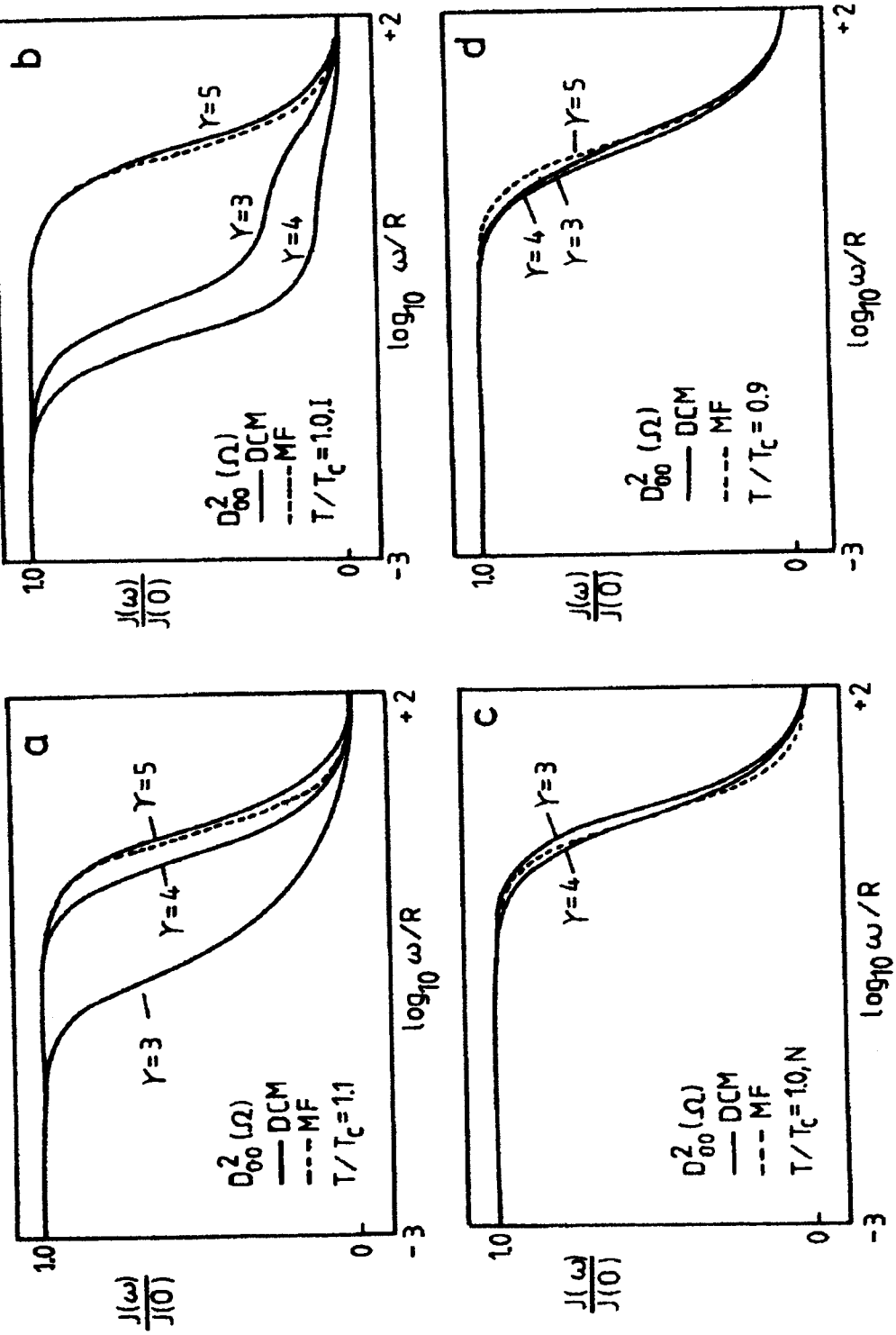

Fig. 15: Dimensionless spectral densities $J(\omega)/J(0)$ vs. dimensionless frequency ω/R plotted logarithmically for the dynamic cluster model; a) $T/T_c = 1.1$, i.e. in the isotropic phase above the liquid crystal phase; b) $T/T_c = 1.0$, in the isotropic phase at the phase transition; c) $T/T_c = 1.0$, in the liquid crystal phase at the phase transition; d) $T/T_c = 0.9$, deep in the liquid crystal phase. Dashed line is the mean field result and solid lines are for $\Gamma = 3,4$, and 5 cluster particles.

VII. Molecular Dynamics at the Nematic to Smectic A-Phase Transition

A) Experiments

We studied in considerable detail the N/S_A phase transition with several nitroxide probes in two different liquid crystalline solvents: 40,6 and a mixture of 80CB-60CB, which exhibits a re-entrant nematic phase [31,52-54]. Our X-band ESR spectrometer is designed for milliKelvin temperature control. What we measure are the ESR linewidths δM of the three hyperfine lines (due to ^{14}N), and we study B and C, which are appropriate linear combinations of them (i.e. $\delta M = A + BM + CM^2$, where M is the z-component of ^{14}N spin). These show divergences at the various phase transitions [31,42,54]. We summarize in Tables 2a and 2b critical exponents and their magnitudes, which are obtained by non-linear least squares fits to the data after one subtracts off the background widths due to spin relaxation associated with the overall reorientation. For the smaller probes PDT and MOTA (cf. Fig. 8),we observe a universal result in the nematic phase, just above the SmA phase, viz. a critical exponent of $\gamma = -1/3$, within experimental error.

However, the larger spin probe P-probe showed no discernable critical effect at this transition in the nematic phase. On the other hand, it did show a critical exponent of $-.22 \pm 0.03$ on the smectic phase side of this transition in 40,6 solvent (the only solvent studied with this probe); whereas PDT and MOTA show no clear critical effect, only a weak hint of a pre-transitional anomaly on the smectic phase side.

The re-entrant nematic-smectic ($RN-S_A$) transition in 60CB-80CB was also studied, and it showed a critical exponent of nearly -1/3 for PDT but only -0.13 for MOTA on the smectic side of this phase transition. Again, there is only a weak hint of a pre-transitional anomaly on the re-entrant nematic side.

Critical-type divergences are also observed on both sides of the I-N transition. The I-N phase transition is characterized (on either side) by spin relaxation parameters which diverge with exponent close to -1/2 as is consistent with a Landau - de Gennes mean-field theory of fluctuations in the orientational order parameter [55]. This results in a slowly-fluctuating orientational potential at the site of the probe molecule, which is able to modulate the rotational reorientational of the probe, thereby leading to the observed critical-type of effect on the spin relaxation [30,55]. Our virtually universal observations of -1/2 for the critical exponent on either side of the I-N transition is in support of the reliability of the technique.

While the weak first order I-N phase transition is generally well-characterized by mean-field theory, this is not so for the $N-S_A$ transition, which is most likely second-order for 40,6 [56] and to which scaling lawas analogous to the λ-transition in He have been applied [57,58]. In the dynamic scaling approach of Brochard [58] and of Jähnig and Brochard [59], the coherence length ξ characterizing fluctuations in the smectic order parameter $\psi(\vec{r},t)$, which is complex, is predicted to diverge as $(T-T_c)^{-0.66}$

Table 2a: CRITICAL EFFECTS: 4O,6

	PDTempone		MOTA		P-Probe	
	B	C	B	C	B	C
			ISOTROPIC PHASE (Nr. Nematic)			
k:	7.6 ± 1.7	17.4 ± 2.1	58 ± 5	68 ± 6	161 ± 49	66 ± 37
γ:	-0.49 ± 0.11	-0.45 ± .09	-0.47 ± .02	-0.50 ± .02	-0.49 ± .12	-0.50 ± .15
			NEMATIC PHASE (Nr. Isotropic)			
k:	4.46 ± .05	9.7 ± 0.2	43.0 ± 0.15	44.0 ± 0.2	210 ± 1	125 ± 1.5
γ:	-0.48 ± .01	-0.54 ± .02	-0.48 ± 0.01	-0.50 ± 0.01	-0.51 ± 0.1	-0.49 ± .02
			NEMATIC PHASE (Nr. Smectic A)			
k:	4.1 ± 1.7	6.0 ± 0.8	8.0 ± 0.2	5.2 ± 0.4	No Critical Effects Observed	
γ:	-0.33 ± .07	-0.38± 0.06	-0.32 ± 0.01	-0.33 ± 0.02		
			SMECTIC PHASE (Nr. Nematic)			
k:	No Critical Effects Observed		No Critical Effects Observed		713 ± 3	702.8 ± .7
γ:					-0.21 ± .03	-0.23 ± .02

Above Based on Fits to Form
$B,C = k(T-T^*)^{\gamma}$ (in mG.)
Errors shown are from the non-linear least squares fits
(From Ref. 52)

Table 2b: CRITICAL EFFECTS: 6OCB - 8OCB

	PDT		MOTA	
	B	C	B	C
ISOTROPIC PHASE (Nr. Nematic)				
k:	14 ± 2	46 ± 2	42 ± 5	39 ± 16
γ:	-0.43 ± .09	-0.40 ± .03	-0.48 ± 0.08	-0.48 ± 0.04
NEMATIC PHASE (Nr. Isotropic)				
k:	16.2 ± .03	29.9 ± .03	No Critical Effects Observed	
γ:	-0.50 ± .01	-0.56 ± .01		
NEMATIC PHASE (Nr. Smectic A)				
k:	17 ± 3	12.5 ± 1.2	75 ± 8	77 ± 6
γ:	-0.30 ± .02	-0.36 ± .03	-0.36 ± .02	-0.35 ± .02
SMECTIC PHASE (Nr. Re-entr. Nematic)				
k:	19 ± 3	32 ± 3	207 ± 10	262 ± 33
γ:	-0.33 ± .02	-0.38 ± .02	-0.13 ± 0.01	-0.13 ± 0.02

Above Based on Fits to form
$B,C = k(T-T^*)^{\gamma}$ (in mG)
(From Ref. 52)

[66]. The true story is actually more complicated, involving separate critical exponents for $\xi_{\parallel}$ and $\xi_{\perp}$, the coherence lengths parallel and perpendicular, respectively to the nematic director, and these exponents appear to vary from one liquid-crystal to another [56,60].

B) Proposed Model

We have proposed the following model to explain our principal results [31]. As discussed above, the probe has a preference to be located in the lower density regions of the smectic layer, i.e. the alkyl chain region [24]. As the smectic phase is approached from higher temperature, and smectic layering forms as a pre-transitional phenomenon (i.e. cybotactic clusters), there is "expulsion" of the probe to the lower density regions of the transitory smectic layer. Molecular parameters which affect spin relaxation (e.g. the nematic ordering parameters S_p and/or τ_R) are affected by this expulsion effect. The onset of smectic layers near the transition is described by density fluctuations: $\rho(\vec{r},t)$ which also affects the translational motion of the probe. Since the critical fluctuations in $\rho(\vec{r},t)$ occur on a much longer time-scale separation of the two types of motions which simplifies the analysis. Thus, as cybotactic clusters form and break up in different regions, molecular dynamics and therefore the spin relaxation of the probe is modulated.

In our formal approach, we first expand the relevant relaxation parameter Q (= e.g. S_p or τ_R) as a Taylor's series in the deviation of the density from its mean value ρ_0, i.e. $\Delta\rho(\vec{r},t) = \rho(\vec{r},t) - \rho_0$. That is

$$Q(\vec{r}_B,t) = Q_0 + Q_1\Delta\rho(\vec{r}_B,t) + Q_2[\Delta\rho(\vec{r}_B,t)]^2 + \ldots \qquad (25)$$

where the subscript B refers to the location of the probe. The translational diffusion of the probe is taken to obey a Smoluchowski equation with a time-dependent potential [30]:

$$\frac{\partial P(\vec{r}_B,t)}{\partial t} = -\underset{\sim}{\nabla} \cdot \underset{\sim}{D} \cdot \{\underset{\sim}{\nabla} + [\underset{\sim}{\nabla} U(\vec{r}_B,t)]/kT\}P(\vec{r}_B,t). \qquad (26)$$

In Eq. (26) $P(\vec{r}_B,t)$ is the probability density of finding the probe at $\vec{r}_B$ at time t, $\underset{\sim}{D}$ is the translational diffusion tensor with components $D_{\parallel}$ and $D_{\perp}$, while the potential of mean force on the probe is a functional of the density fluctuations, i.e.

$$U(\vec{r}_B,t) = U[\Delta\rho(\vec{r}_B,t)] \; . \qquad (27)$$

Now $\Delta\rho(\vec{r})$ is related to the complex order parameter $\psi(\vec{r})$ in the usual manner [79,80]:

$$\Delta\rho(\vec{r}) = \frac{\rho_0}{\sqrt{2}} \mathrm{Re}\left[\psi(\vec{r}) e^{iq_s z}\right] = \frac{\rho_0}{\sqrt{2}} \left|\psi(\vec{r})\right| \mathrm{Re}(e^{iq_s[z-u(\vec{r})]}). \qquad (28)$$

Here $q_s = \frac{2\pi}{d}$, where d is the smectic layer spacing, and the phase, $q_s u(\vec{r})$ of $\psi(\vec{r})$ locates the smectic layer's density maxima and minima in each part of the sample. If for simplicity we follow dynamic scaling according to Jähnig and Brochard [58.59], we obtain for the $\vec{q}$-th Fourier component of $\psi(\vec{r})$ the time correlation function:

$$\langle\psi^*(\vec{q},t)\psi(\vec{q},0)\rangle = \langle|\psi_{\vec{q}}|^2\rangle e^{-\Gamma_{\vec{q}} t} \qquad (29)$$

$$\langle|\psi_{\vec{q}}|^2\rangle = \frac{k_B T}{2A}\left[(1 + q_\perp^2 \xi_\perp^2 + q_{||}^2 \xi_{||}^2)\right] V^{-1}. \qquad (30)$$

Here $q_{||}$ and $q_\perp$ are the components of $\vec{q}$ parallel and perpendicular (to the nematic director), V is the sample volume, and A is the coefficient in the term quadratic in $\psi(\vec{r})$ in the Landau expansion of the smectic free-energy. (A goes to zero almost as ξ^{-2}). The damping $\Gamma_{\vec{q}}$ of the $\vec{q}$-th mode is given by:

$$\Gamma_{\vec{q}}^{-1} = \frac{\tau_m}{(1 + q_\perp^2 \xi_\perp^2 + q_{||}^2 \xi_{||}^2)^x} \qquad (31)$$

with τ_M a characteristic relaxation time for the cybotactic clusters and $x = 3/4$. The relaxation time τ_m is expected to diverge as $\xi^{3/2} \propto (T-T_c)^{-1}$.

In the spirit of a Landau expansion we consider only the lowest order terms in $\Delta\rho(\vec{r}_B)$ to represent the time-dependent fluctuations in Q. That is:

$$\langle\Delta Q(\vec{r}_B,t)\Delta Q(\vec{r}_B,0)\rangle = Q_1^2 C(t) + \text{H.O.T} \qquad (32)$$

where

$$C(t) = \langle\Delta\rho(\vec{r}_B,t)\Delta\rho(\vec{r}_B,0)\rangle/\rho_0^2 . \qquad (33)$$

The method of approach for calculating $C(t)$ including the critical hydrodynamics of the phase transition and the translational diffusion of the probe is based upon methods we have previously developed [30]. The dominant contribution to the ESR linewidths should be from terms involving $J(\omega) \approx J(0)$ yielding (in the limit $q_s \to 0$):

$$J(0) = \frac{Mk_B T}{8\pi} \frac{z\tau_m}{\xi} (1 + z^{1/2})^{-1}$$

$$\underline{z \cong 1} \quad \frac{Mk_B T}{16\pi} \left(\frac{\tau_m}{\xi}\right) \propto \xi^{1/2} \propto (T-T_c)^{-1/3}$$

$$\underline{z \ll 1} \quad \frac{Mk_B T}{8\pi D} \xi \propto \xi \propto (T-T_c)^{-2/3} \qquad (34)$$

where $z \equiv (1 + D\tau_m/\xi^2)^{-1}$ measures the relative importance of translational diffusion over the coherence length ξ vs. relaxation of the order parameter in providing averaging the fluctuations in Q. Here $z \cong 1$ corresponds to relaxation dominated by director fluctuations, while $z << 1$ corresponds to relaxation dominated by molecular translational diffusion. The limiting form for $z \cong 1$ predicts the experimentally observed critical divergence of -1/3.

In the second case we keep $q_s = \frac{2\pi}{d}$ but introduce other simplifications. Then for J(0) we obtain

$$J(0) = \frac{Mk_BT}{16\pi} \quad \frac{\tau}{\xi} \quad \frac{\sqrt{1+c} - 1}{c} \quad . \tag{35}$$

Here $c \equiv q_s^2 D_{\parallel} \tau_m$ measures the relative importance of averaging out the effects of density fluctuations $\Delta\rho(\vec{r})$ in a <u>single</u> smectic-like layer through diffusion of the probe in the direction normal to the layer vs. the relaxation of the smectic layers. As $c \to 0$, corresponding to probe diffusion being unimportant, one obtains essentially the previous result for $z \approx 1$. For $c >> 1$, $J(0) \propto \tau_m^{1/2}/\xi_{\parallel} \propto \xi^{-1/4}$, and it does <u>not</u> diverge, but rather goes to zero.

Based upon measurements of $\xi_{\parallel}$ [56] and D [52,61,62] we estimate $\xi_{\parallel} \sim 10^{-5}$ cm for $T-T_c = 0.1^oK$ and $D \sim 10^{-6} cm^2/sec$. Also we estimate $\tau_m \sim 10^{-5}$ to 10^{-6} sec at $T-T_c = 0.1^oC$ [31], so $D_{\parallel}\tau_m/\xi^2 \sim 10^{-2}$ to 10^{-1} (for $T-T_c \sim 0.1^oC$), while $D_{\parallel}\tau_m q_s^2 \sim 10$ to 10^2. Thus, while it may be reasonable to ignore the averaging effects of translational diffusion over the distance of ξ_1, this is questionable for diffusional averaging over a single smectic layer of thickness d.

However, the above simple model, i.e. Eq. (32), implicitly ignores the potential of mean force $U(\vec{r}_B,t)$ in Eq. (26). If U is a very sensitive functional of $\Delta\rho(\vec{r})$ (cf. Eq. (27)), then as $\Delta\rho(\vec{r})$ diverges as the critical point is reached, Eq. (26) would predict virtually no diffusion parallel to the normal to the smectic phases in the cybotactic clusters. Instead, the probe would reside entirely in the alkyl chain regions in such clusters, i.e. the "expulsion effect" referred to above. Thus, the modulation of the parameter Q would be primarily determined by the formation and break-up of the cybotactic clusters, with the probe rapidly adjusting its location within the layers accordingly. This effect would be measured by the correlation function: $\langle\psi(r_B,t)\psi(r_B,0)\rangle$ and we would obtain Eq. (34) for the (simplified) spectral densities.

Our model for cooperative molecular dynamics and critical effects at the N-S phase transition is still a rather simple one, and we have not yet explicitly considered the role of a finite $U[\Delta\rho(\vec{r}_B,t)]$ despite its presumed importance. On the other hand, we recall the Moro-Nordio theory [35] for spin-relaxation within the smectic phase. These two theoretical analyses are really related to one another. The more general approach would yield smectic-like fluctuations experienced by the spin probe near the

N-S phase transition, but a well-defined smectic-like potential deep in the smectic phase. It may be written in terms of a potential with the following form:

$$U[\beta,\Delta\rho(\vec{r}_B)] = AY_0^2(\beta) + B'[\Delta\rho(\vec{r}_B)]Y_0^2(\beta) + C'[\Delta\rho(\vec{r}_B)] \ . \qquad (36)$$

If we assume that $B'[\Delta\rho(\vec{r}_B)]$ and $C'[\Delta\rho(\vec{r}_B)]$ are linearly proportional to $\Delta\rho(\vec{r}_B)$, then deep in the smectic we can let $B' \propto \frac{\rho_0}{2}|\psi_0|\cos\frac{2\pi}{d}z$ so that $B' = B\cos\frac{2\pi}{d}z$ (and similarly for C'). This is just the form Moro and Nordio use (cf. Eq. (8)). This suggests that near the phase transition we should use as an explicit form for $U[\Delta\rho(\vec{r}_B),t]$:

$$U = AY_0^2(\beta) + B'\Delta\rho(\vec{r}_B)Y_0^2(\beta) + C''[\Delta\rho(\vec{r}_B)] \qquad (36)$$

in conjunction with the Fourier analysis of $\Delta\rho(\vec{r}_B)$ outlined above.

Such a model would more explicitly describe how the probe ordering and combined rotational-translational dynamics is modulated by the smectic-like pre-transitional fluctuations. It may also enable one to correlate observations at the N-S phase transition with SRLS type of behavior deep in the smectic phase.

VIII. Translational Diffusion

Our primary motivation here is to obtain the translational diffusion coefficients for the probe in liquid crystals in conjunction with studies of cooperative rotational dynamics and phase transition studies. The mechanism of Heisenberg Spin exchange can be used to study translational diffusion over molecular dimensions, while the new ESR imaging technique measures diffusion over macroscopic dimensions and can detect anisotropies in the diffusion coefficient.

A) Heisenberg Spin-Exchange

Our results [52,61] with PDT (cf. Fig. 16) show trends that are consistent with the model we have proposed [24] that in mono-layer smectics like 40,6 the PDT probes are gradually "expelled" from the central aromatic core regions to the aliphatic chains as one proceeds to lower temperature phases; but for cyanobiphenyls the probe expulsion takes place prior to the formation of the smectic mesophase, as is evidenced by translational diffusion coefficients, which show no discontinuities (in magnitude or activation energy) at the phase transitions in the latter case. Also the low activation energy of about 2.5 kcal/mole for 6OCB-8OCB and the decreasing activation energy of 4.7 to 1 kcal/mole for 40,6 are more characteristic of diffusion through aliphatic chains. This emphasizes the important role such studies can play in developing an understanding of motional dynamics.

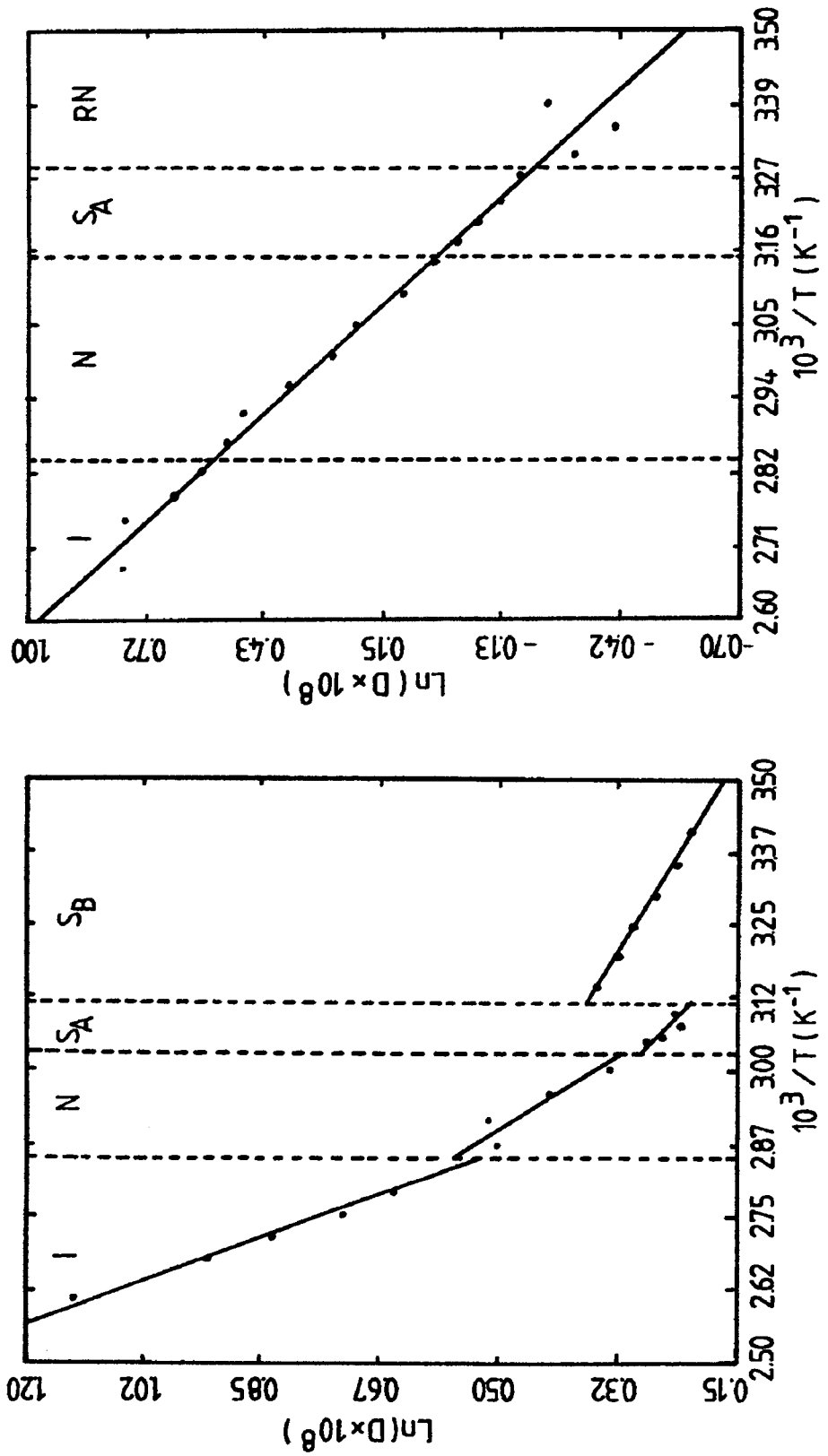

Fig. 16: Diffusion coefficients obtained from Heisenberg spin-exchange for PD-Terpone in liquid crystals: a) 40,6 and b) 8OCB-6OCB mixture. $\ln(D \times 10^6)$ vs. $10^3/T$ is plotted, where D is in units of $cm^2 s^{-1}$. (From Ref. [63].)

B) ESR Imaging and Macroscopic Diffusion

The relaxation techniques for measuring translational diffusion as discussed above for HE are based on bimolecular collisions of spin probes. As such, they measure diffusion over dimensions of (several) molecular length(s). However, they do not provide direct means for measuring diffusional anisotropy. Also, the analysis leading to the diffusion coefficient depends upon the choice of molecular model. It is therefore useful to have measurements of diffusion that do not depend upon one's choice of model and that can be used to study anisotropiy in diffusion. Such studies could then be compared with the sub-microscopic ones to understand much better the nature of the molecular model.

We have developed a technique employing ESR imaging, which we have found to be convenient for measurement of D in the range of $10^{-8}<D<10^{-5}$ cm^2/sec, and we have succeeded in measuring the anisotropy of D in the liquid crystal 5,4 where $D \gtrsim 5 \times 10^{-7}$ cm^2/sec [32]. In the nematic phase we find $D_{\parallel}/D_{\perp} = 0.71 \pm 0.1$ which is consistent with a pre-transitional smectic-like effect [33] that could be expected, since 5,4 does exhibit a N-S transition.

Utilization of such an imaging technique to study the anisotropic translational diffusion properties of the various smaller and larger spin probes in the different liquid crystalline phases would be useful for comparing with studies of sub-microscopic rotational dynamics (and sub-microscopic translational dynamics). Also one might hope to observe pre-transitional anomalies at the liquid crystalline phase transitions (e.g. a decrease in $D_{\parallel}$ as the N-S_A phase transition is approached from the nematic phase, cf. Ref. [31]).

IX. Rotational Dynamics in Model Membranes

A) Dynamic Molecular Structure and Phase Transitions in Lipid Multilayers

The use of defect-free oriented samples enabled us to clearly observe lipid phase transitions through the appearance of composite spectra in the transition (two-phase) region [63]. From ESR observations on low-water content DPPC and DMPC (cf. Fig. 17) three phase transitions were found over a temperature range below 180°C: two were assigned to the main transition and to the isotropic transition by reference to the transition temperatures in the literature. The remaining one, at 100-110°C, was characterized as a "chain-orientational" transition.

The ordering and the rotational diffusion tensor of the various spin labels could be determined accurately as a function of temperature, % H_2O, and phase (e.g. Table III). CSL, 5PC, and 16PC exhibit in all phases decreasing order parameters S, according to CSL > 5PC > 16PC and increasing motional rate (measured by $\bar{R}$ the mean rotational diffusion coefficient) again according to CSL < 5PC < 16PC, while the anisotropy in rotational motion obeys CSL < 5PC < 16PC, consistent with the well-known concept of the increased flexibility as one proceeds down the chain [64]. However, we have been

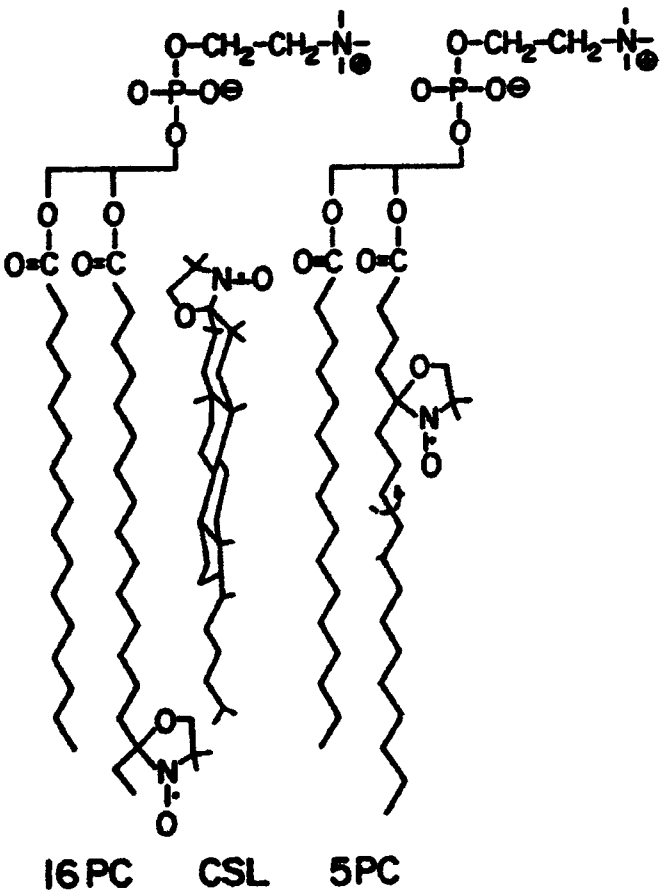

Fig. 17: Schematic structures of CSL, SPC, 16PC (from Ref. [63]).

able to quantify this flexibility gradient in terms of its reduced ordering and its symmetry, as well as the increased motional rate [63].

Using these results we can characterize the main (or gel-to-Lα(1)) transition as primarily a "chain-diffusional" transition, while, as noted above, the new high-temperature one is characterized as a "chain-orientational" transition: the ordering parameter S experiences a more significant relative reduction at the second transition compared to that at the main transition, whereas the diffusion coefficient $R_\perp$ for the chain probes (i.e. 5PC and 16PC) experiences a more significant relative increase at the main transition. Thus, a relatively smaller reduction in molecular ordering more effectively "unfreezes" the chain motions at the main transition compared to the second one. The relative increase in $R_\perp$ for CSL at the two transitions is, however, comparable suggesting that while local chain motion increases more significantly at the main transition, the overall molecular motions exhibit comparable relative changes at both phase transitions. Also, whereas $R_\perp$ shows substantial change at the phase transitions, $R_\parallel = NR_\perp$, which measures the motion about the long chain axis, is much less affected. This undoubtedly reflects the existence of significant motion of this type in the gel phase, which may be due to its relatively unhindered nature. Finally, we find that at

Table III: Parameters for Molecular Ordering and Anisotropic Rotation of CSL in DPPC[d]

t, °C	phase	$(D^2_{00})^d$	$(D^2_{02}+D^2_{0-2})^d$	$R_\perp$, [c] s^{-1}	$R_\parallel$, [c] s^{-1}	N	E_a, kcal/mol	τ_2^{*-1}, G
			(A) Hydrated to 3 wt %					
40	I	0.90	-0.01	$2.9\ 10^5$	$4.4\ 10^7$			
50		0.90	-0.01	$4.0\ 10^5$	$6.0\ 10^7$	150	7.7	1.5
60		0.90	-0.01	$6.2\ 10^5$	$9.3\ 10^7$			
70		0.90	-0.01	$8.3\ 10^5$	$1.2\ 10^8$			
80	II	0.76	-0.03	$6.8\ 10^6$	$3.4\ 10^8$			
85		0.73	-0.03	$8.0\ 10^6$	$4.0\ 10^8$	50	(8.7)	1.2
90		0.67	-0.03	$9.6\ 10^6$	$4.8\ 10^8$			
110	III	0.28	0.08	$1.1\ 10^8$	$1.7\ 10^9$			
120		0.21	0.06	$1.5\ 10^8$	$2.4\ 10^9$			
130		0.14	0.03	$2.0\ 10^8$	$3.2\ 10^9$	16	9.2	1.0
140		0.13	0.03	$2.5\ 10^8$	$4.0\ 10^9$			
160	IV	0	0	$5.8\ 10^8$	$2.9\ 10^9$			
170		0	0	$6.7\ 10^8$	$3.4\ 10^9$			
180		0	0	$7.5\ 10^8$	$3.8\ 10^9$	5	5.0	1.0
			(B) Hydrated to 7 wt %					
40	I	0.88	-0.005	$3.0\ 10^5$	$4.5\ 10^7$			
50		0.88	-0.005	$5.0\ 10^5$	$7.5\ 10^7$			
60		0.88	-0.005	$7.0\ 10^5$	$10.5\ 10^7$	150	(8.7)	1.5
70	II	0.78	-0.007	$9.0\ 10^6$	$4.5\ 10^8$			
80		0.74	-0.009	$1.2\ 10^7$	$6.0\ 10^8$			
90		0.65	-0.015	$1.6\ 10^7$	$8.0\ 10^8$	50	(7.0)	1.2

[a]Estimated errors: ±2% in (D^2_{00}), ±30% in $(D^2_{02}+D^2_{0-2})$, ±10% in $R_\perp$, ±20% in N, ±20% in E_a, and ±01. G in τ_2^{*-1}. Note $R_\parallel = NR_\perp$. [b]I, biaxial gel phase; II and III, liquid-crystalline phases; IV, isotropic phase. [c]Correlation times: $\tau_\perp = 1/6R_\perp$, $\tau_\parallel = 1/6R_\parallel$, and $\bar{\tau} = 1/6\bar{R} = 1/6(R_\parallel R_\perp)^{1/2}$. [d]The relationship between (D^2_{00}) and λ and ρ is given by the following expression:

$$(D^2_{00}) = \int_{\phi'}\int_{\theta'} P(\theta',\phi')1/2(3\cos^2\theta' - 1)\sin\theta'\, d\theta'\, d\phi'$$

and $(D^2_{02}+D^2_{0-2}) = \int_{\phi'}\int_{\theta'} P(\theta',\phi')(6^{1/2}/2)\sin^2\theta' \cos2\phi' \sin\theta'\, d\theta'\, d\phi'$, where θ' denotes the angle beteen the principal axis z' of the ordering tensor and the principal axis z" of the director frame. $P(\theta',\phi')\sin\theta'\, d\theta'\, d\phi'$ is the distribution of z' relative to z" given by $P(\theta',\phi') \propto \exp[-1/2(3\cos^2\theta' - 1) + (6^{1/2})\rho \sin^2\theta' \cos2\phi']$. (From Ref. [65].)

both phase transitions there is a more significant relative reduction in ordering at the end of the chain but a smaller increase in fluidity (as measured by $R_{\perp}$). Thus while there is greater "melting" of orientational order at the end of the chain, the end-chain motions are not as significantly tied to the ordering.

B) Lipid-Gramicidin Interactions

Given that the ESR spectra from dispersions is somewhat ambiguous to interpret, we adapted our alignment methods of sample preparation to prepare very well-aligned uniform samples containing the stable polypeptide gramicidin A (DA). This polypeptide is frequently used to mimic the effects of protein on phospholipid bilayers [65]. Its advantages are its known chemical structure and its known helical conformations, its considerable stability, and its ready availability. Chapman and co-workers have found that the dimeric GA is incorporated into the lipid bilayer, and they regard it as a model for the interactions of the polypeptide segments of transmembrane proteins within the hydrocarbon regions of the lipid bilayers [65].

Our principal findings are the following [66]: 1) In the gel phase we observed distinct two-component spectra which could be assigned to highly oriented bulk lipids and to a disordered component, and the latter was fit by a model of "molecular disorder" such that the ordering of these molecules is greatly reduced, but its rotational-motional properties are not appreciably changed (cf. Figs. 18A and 19A). The disordered region at lowest concentration of GA is estimated to consist of about 30-40 lipid pairs, or about five times the number required to coat the GA dimer. This corresponds to a disordered region in the bilayer extending radially about 3 lipid molecules. This effect of disordering is significantly reduced by increasing the wt.% of water, but it appears to be independent of temperature. 2) In the liquid crystalline phase, heterogeneity is not distinguished from the ESR spectrum. Instead, the primary effect of GA is to significantly reduce the observed ordering of all the lipids, with only a very small decrease in motional rates (cf. Figs. 18B, 19B). However, in the high-temperature weakly-ordered phase, addition of GA actually leads to significant increase in ordering. This increase in ordering is also observed in high-water-content dispersions in the liquid crystalline phase. There is no hint of features usually assigned to "immobilized" species in any of the spectra obtained from well-aligned samples However, such features are present in dispersion samples of 4 M% GA prepared from the same materials as the well-aligned ones. If we associate these spectral features with "trapped lipids" due to aggregation of GA, then it follows that microscopically well-aligned samples do not allow for such aggregation.

We conclude from these findings that the principal lipid-GA interaction is that of a boundary effect such that the GA induces disorder in the low-temperature and low water content lipids, but it induces order for high-temperature and high water content (i.e., less ordered) lipids. It has only slight effects on lipid fluidity, in general reducing only slightly the rates of rotational reorientation.

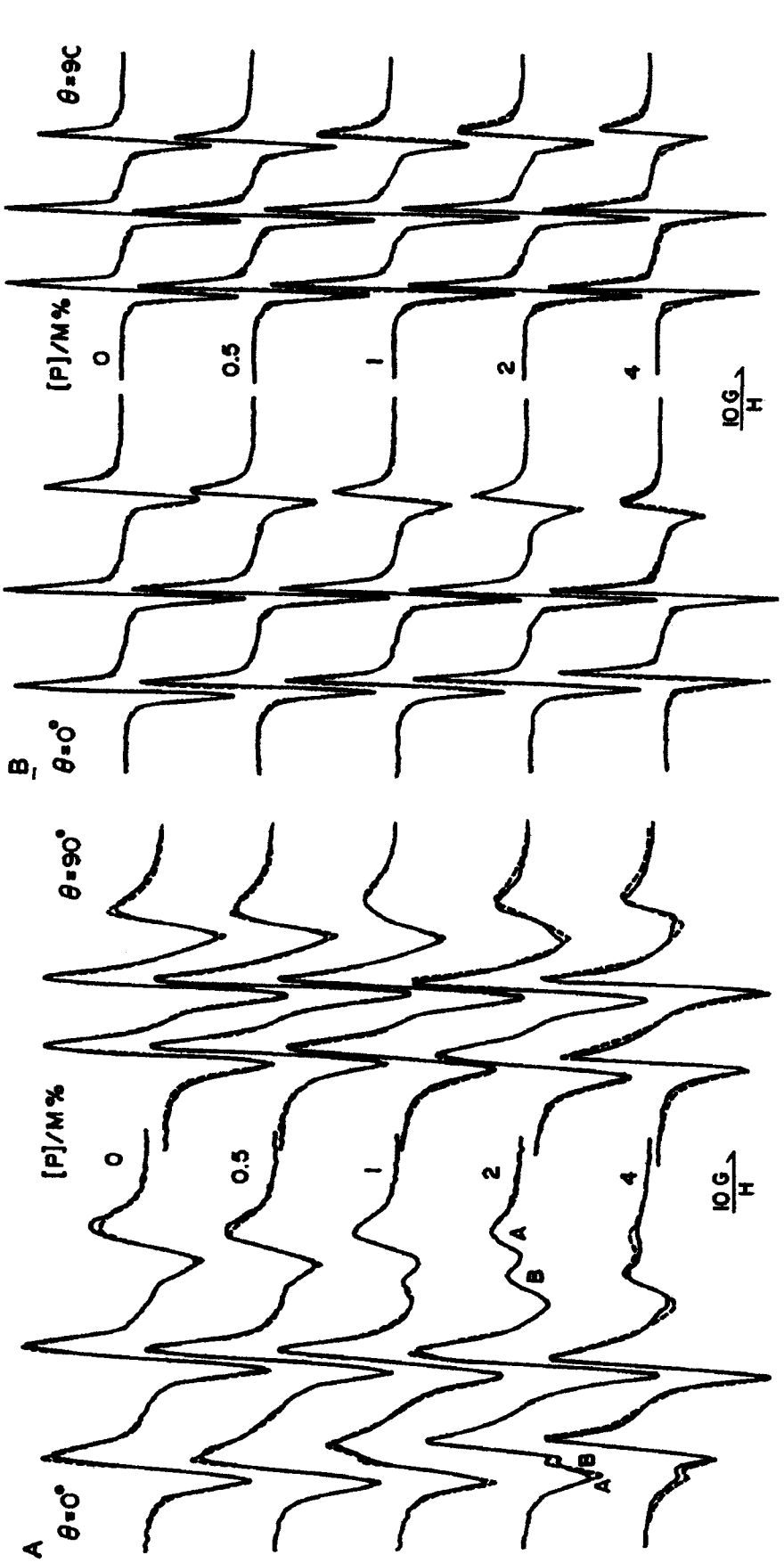

Fig. 18: ESR spectra from 16PC in DPPC hydrated to 7 wt. % for concentrations of GA ranging from 0 to 4 M%. Spectra are shown for $\theta = 0^{\circ}$ and 90°: (A) 50°C corresponding to phase I; (B) 80°C corresponding to phase II. Dashed spectra are simulations. In (A) the ordered and disordered components are labeled A and B respectively. (From Ref. [66].)

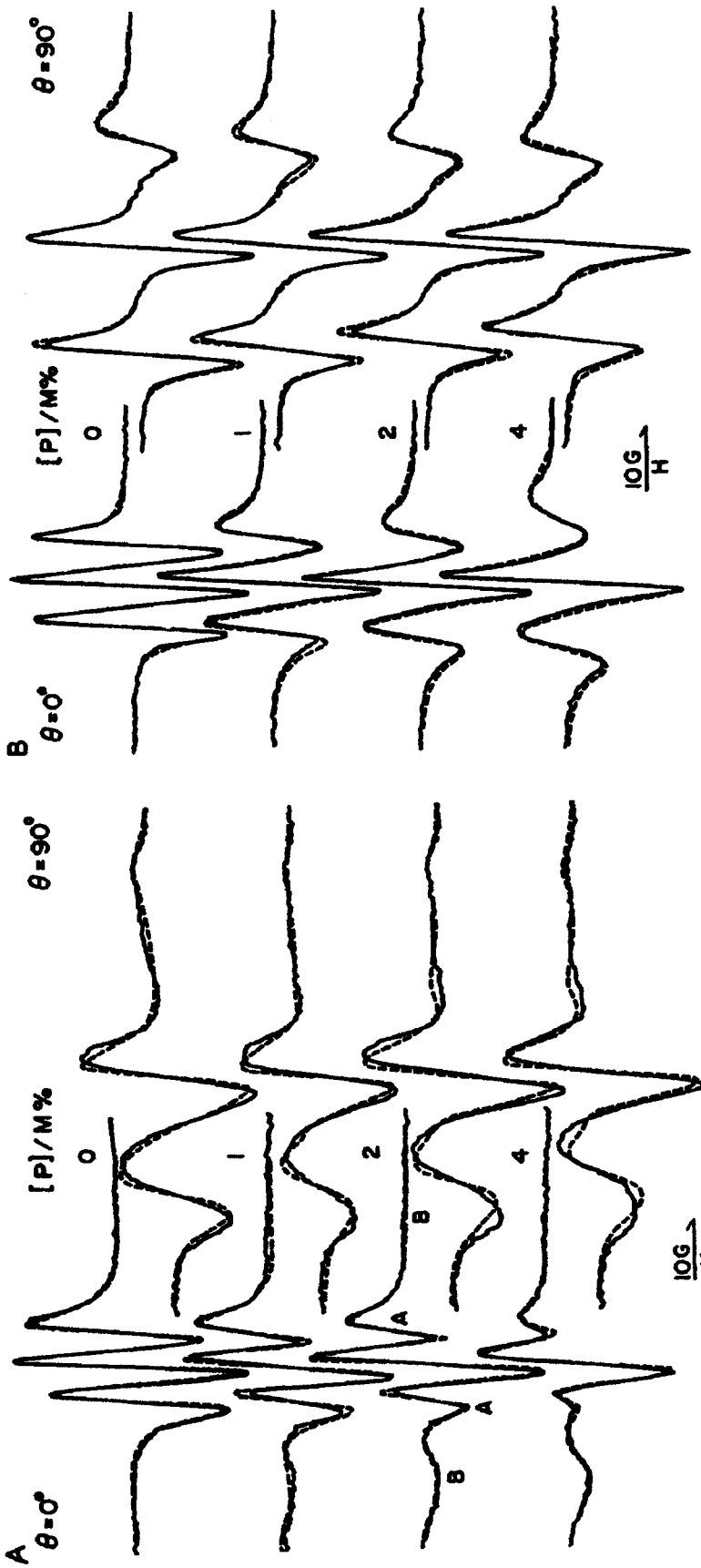

Fig. 19: Same as Fig. 18 but for CSL in DPPC. (From Ref. [66].)

We believe that these various effects can be explained as the consequence of two competing features of the lipid-GA interaction: a "disordering feature" and a "hardening feature". The former induces a disordering of the lipids in their vicinity, while the latter makes them more solid-like, as exemplified by somewhat reduced fluidity and by increasing the order. Furthermore, we require that disordering is dominant under conditions of low fluidity, while hardening is dominant when there is high fluidity. The notion of two apparently opposite effects of the macromolecule on the ordering of lipids has been incorporated into a simple model by Jähnig [67]. He proposed that the ordering at the boundary of a protein should be lower than that for the "ordered" phase but greater than that for the "fluid" phase. Our low water content results are consistent with this model when we apply it to the $L\alpha(1)$ to high-temperature-liquid-crystal phase transition.

The heterogeneity induced by GA at very low concentrations is a distinctly different phenomenon from the one usually assigned to "immobilized" or "trapped" lipids. The clear discrimination of the heterogeneity in the bilayer induced by the GA, and the determination of the molecular properties of this heterogeneity should be significant in understanding the polypeptide - lipid interaction.

X. Electron-Spin Echoes and Rotational Relaxation

It is our expectation that over the next several years the modern electron-spin echo (ESE) technique will become increasingly important in the study of spin relaxation and rotational dynamics. The possibilities have been greatly enhanced by instrumental developments in several laboratories around the world including our own [4, 68-73].

The principal motiovations for applying ESE techniques to spin relaxation studies include: (1) the ability to separate homogeneous from inhomogeneous contributions to the linewidths (or T_2) as well as to profit from the resulting increase in resolution; (2) the ease of simultaneously performing T_1 measurements; (3) the possibility that special ESE techniques could provide information on motional dynamics in addition to that from cw-studies; and (4) the possibility of extending the range of study to slower motions.

(A) ESE and Slow Motional Theory

While ESE work on nitroxides in liquids showed good agreement with the motionally-narrowed line widths extracted by cw-techniques, we were especially motivated by the initial observation [74] that in the slow motional regime, for $\tau_R \sim 10^{-7}$ to 10^{-6} sec, the phase memory time, T_M was found to be proportional to $(\tau_R)^{\alpha}$ with $\alpha \sim 1$ (cf. Fig. 20). Simple arguments suggest this was to be expected. That is, in the slow motional regime, reorientational jumps should lead to spectral diffusion wherein each jump takes place between sites of different resonance field. This would be an uncertainty-in-lifetime broadening that is analogous to the slow exchange limit in the

classic two-site case, and it contributes to T_M. The broadening would then be given by τ_R^{-1}, the jump frequency. This result suggested that studies of the ESE T_M in slow-motional spectra would supply complementary information on motional dynamics to cw-lineshape studies.

A rigorous theoretical basis for the analysis of slow-motional ESE was developed in order to interpret such experiments with confidence [75]. It is based on the same stochastic Liouville equation (SLE) which is used to predict cw-lineshapes (cf. Sect. VI). This emphasizes that echoes relate to the same type of motional effects as do the cw-lineshapes.

Our theoretical results on simple $90^0 - \tau - 180^0 - \tau$ echoes demonstrated that [75]: 1) the ESE decay envelopes show a short-time behavior with an $e^{-C\tau^3}$ dependence on τ and a long-time behavior of $e^{-\tau/T_M^\infty}$. 2) The asymptotic phase-memory decay constant T_M^∞ shows a significant dependence on models, and this was traced to the different

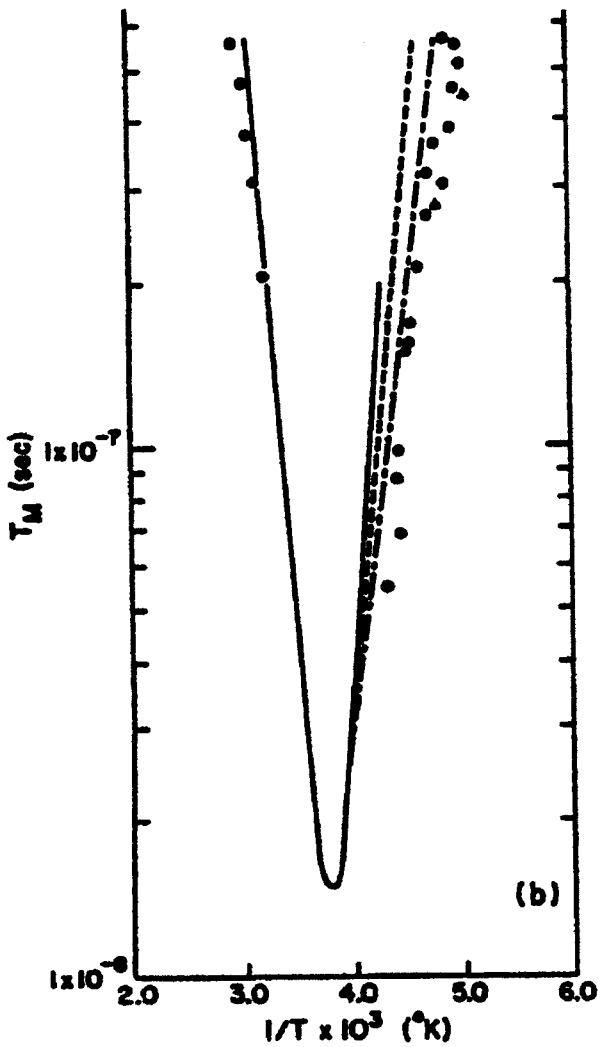

Fig. 20: Graph of T_M (or T_2) vs. T^{-1} for PD-Tempone in 85% glycerol/15% water. The circles show T_M data. The triangles show the T_M from 2D ESE. The different lines represent T_M in the central spectral regime calculated for the models of jump diffusion (solid line), free diffusion (dashed line), and Brownian diffusion (dashed-dotted line). The calculations employed the values of τ_R extrapolated from the motional narrowing regime. (From Ref. [76a].)

mechanisms of spectral diffusion induced by these models. 3) The T_M obtained from selective echoes on different parts of the (nitroxide) spectrum show significant differences. 4) The short-time behavior yields a $c \propto \tau_R^{-1}$, and c is independent of diffusion model.

We also showed that in an ideal two-pulse ESE experiment, the decay envelope is described by [75]:

$$S(\tau) = \mathrm{Re} \sum_{1,j} a_{1,j} \exp [\Lambda_1 + \Lambda_j^*]\tau \qquad (38)$$

which is the real part of a sum of complex exponential functions. The relevant parameters are determined from the SLE, and the Λ_j are the eigenvalues of the stochastic Liouville operator in the rotating frame. Their imaginary parts (i.e. $\mathrm{Im}\Lambda_j = \omega_j$) represent the resonance frequencies of the associated "dynamic spin packets", while the real parts (i.e. $\mathrm{Re}\Lambda_j = T_{2,j}^{-1}$) represent their natural or homogeneous widths and are associated with the observed T_2. The relative contribution of the various spin packets depends upon the coefficients $a_{1,j}$, also provided by the theory. One finds from the simulations that the nitroxide slow-motional cw-spectrum will typically consist of 50-200 such spin packets which make significant contributions. These spin packets overlap with one another (especially when the inhomogeneous width is included), and the typical broad envelope, i.e., the cw-spectrum, is observed. Thus if the $\mathrm{Re}\Lambda_j$ are different in magnitude from one another, one may expect to observe a T_2 that varies across the spectrum. We have developed a two-dimensional ESE technique specifically designed to study variations of the natural width across the spectrum.

A) Two-Dimensional ESE

In our original experiments [76,77], we utilized a standard 90^0-τ-180^0 two-pulse echo sequence and monitored the echo height at 2τ while slowly sweeping through the ESR spectrum by sweeping the dc-magnetic field. This generates an "echo-induced ESR spectrum" for each value of τ. The resonant microwave field H_1 is kept small enough that it does not introduce any distortion into the echo-induced field-swept ESR spectrum (i.e., $\gamma_e H_1 \ll \Delta\omega_s$, where $\Delta\omega_s$ is a measure of the width of spectral detail in the cw-spectrum). After collecting a family of such spectra, a Fourier transform with respect to τ is performed at each field value. The resulting 2D spectrum yields the inhomogeneously broadened absorption-like echo-induced ESR spectrum in one dimension and the homogeneous lineshape in the other dimension. The two-dimensional spectrum is given by:

$$S(\omega,\omega_0) \propto \sum_j a_{j,j} \frac{T_{2,j}}{1+\omega^2 T_{2,j}^2} \exp[-2\tau_d/T_{2,j}]\exp[-(\omega_0-\omega_j)^2/\Delta^2] \qquad (39)$$

where $\omega_0 = \gamma_e H_0$ and a Gaussian inhomogeneous broadening of width Δ has been assumed, and we have included the effect of the finite dead-time τ_d. Note that for

$\omega = 0$ we almost recover the expression for an ESR-like absorption spectrum with Gaussian inhomogeneous broadening. Along the ω-axis one observes a blend of Lorentzian line-shapes from the various "dynamic spin packets". In general, we find that while T_2 varies across the spectrum, the observed 2D-ESE line-shape at each position ω_0 is close to a simple Lorentzian in ω. Examples of such 2D-ESE spectra appear in Fig. 21.

It is preferable, however, to study the normalized contours to obtain useful information. This representation is developed by dividing every slice of the spectrum along the "width" (or ω)-axis by its corresponding amplitude at 0 MHz and then generating contour lines at every 10% change in height. The resulting map reveals the homogeneous line-shape as a function of field location unaffected by differences in signal height. One finds that these contours are very sensitive not only to the rate of reorientation but also to the model of molecular reorientation, (e.g. whether it is by jumps, free diffusion, of Brownian motion) with different characteristic patterns for each! We show in Fig. 22 an actual experimental demonstration of the sensitivity to motional anisotropy by comparing the results for tempone, which tumbles nearly isotropically vs. those for CSL, whose motion is anisotropic. While the T_2's are comparable, the shapes are significantly different, emphasizing the large anisotropy for CSL.

It should also be emphasized that Fig. 22 shows patterns that are consistent with a Brownian reorientation model, since jump models predict parallel contours with no features [76a].

We have already applied the 2D-ESE technique to oriented lyotropic liquid crystalline samples [76b] (cf. Fig. 21). In Fig. 23, we show a sequence of experimental contours from oriented multilayers of low water-content DPPC-doped with CSL for different temperatures and angle of tilt θ, and in Fig. 24 we show typical simulations which relate to these results showing specific sensitivities to the orienting potential as well as details of the dynamics.

We wish to emphasize the importance of the latter. Our studies with the CSL spin-label in the oriented samples (cf. Section IX) have shown that even in the slow-motional region, where cw-spectral simulations are only slightly sensitive to motion, it is very difficult to obtain a unique set of parameters characterizing the system under study. The 2D-ESE results are much more sensitive to these matters as illustrated in the simulations of Figs. 25. In Fig. 25a we show a cw-ESR simulation for high ordering ($S = 0.87$) and very slow motion $R \approx 10^4$ sec^{-1}. We superimpose the results for isotropic ($N = 1$) and very anisotropic ($N = 100$) motions to demonstrate that they are almost indistinguishable. However, in Fig. 25b we show the 2S-ESE contours and 0 MHz slices for the same parameters. They clearly differ both in magnitude and shape and are very easily distinguishable!

As described above, the 2D-ESE spectrum is obtained by monitoring the height of a spin echo from a two-pulse sequence, as the magnetic field is scanned.

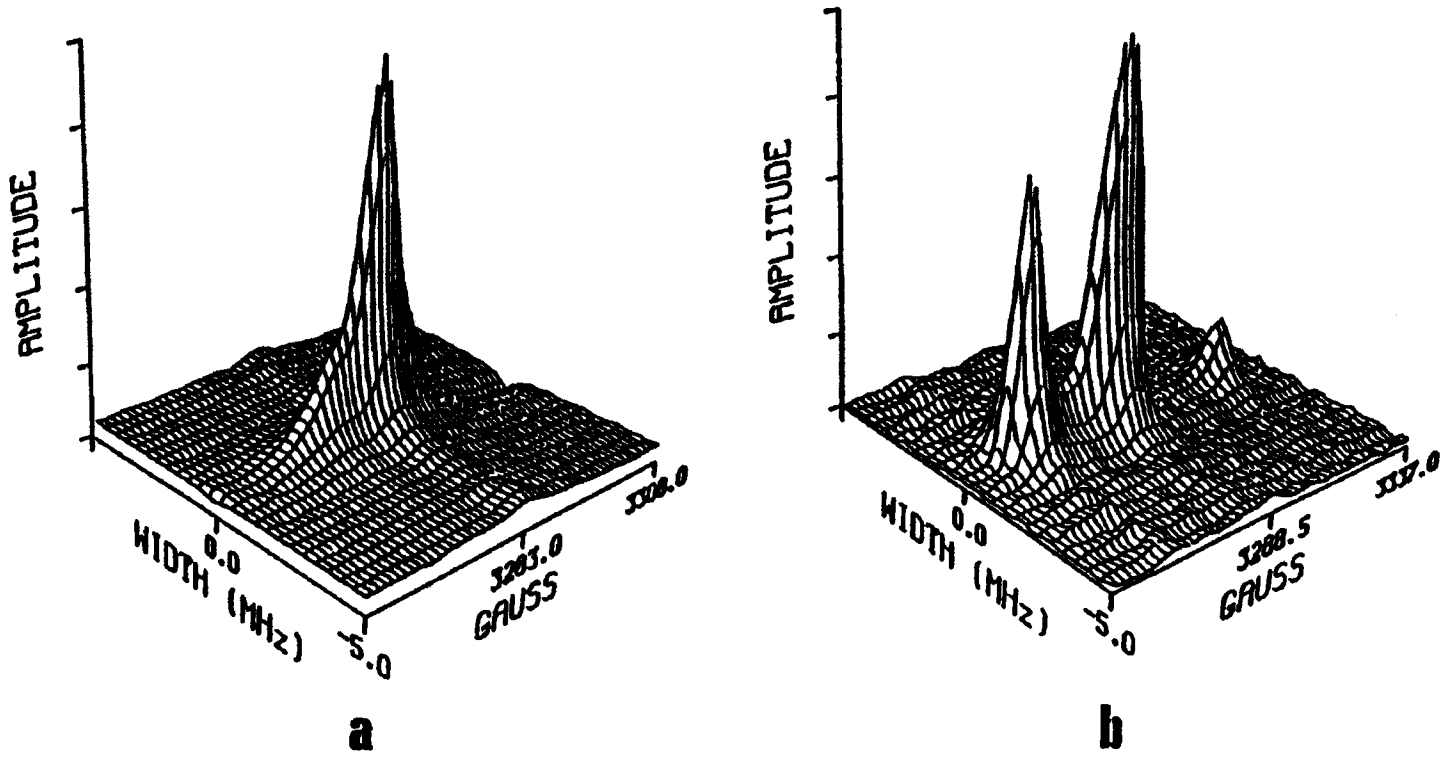

Fig. 21: Experimental 2D-ESE spectra from CSL spin probe in oriented multilayers of low water content DPPC: a) $\theta = 0^{o}$ $T = -20^{o}C$ b) $\theta = 90^{o}$ $T = -20^{o}C$ where θ denotes the orientation of the director with respect to the external and applied magnetic field H. (From Ref. [76b].)

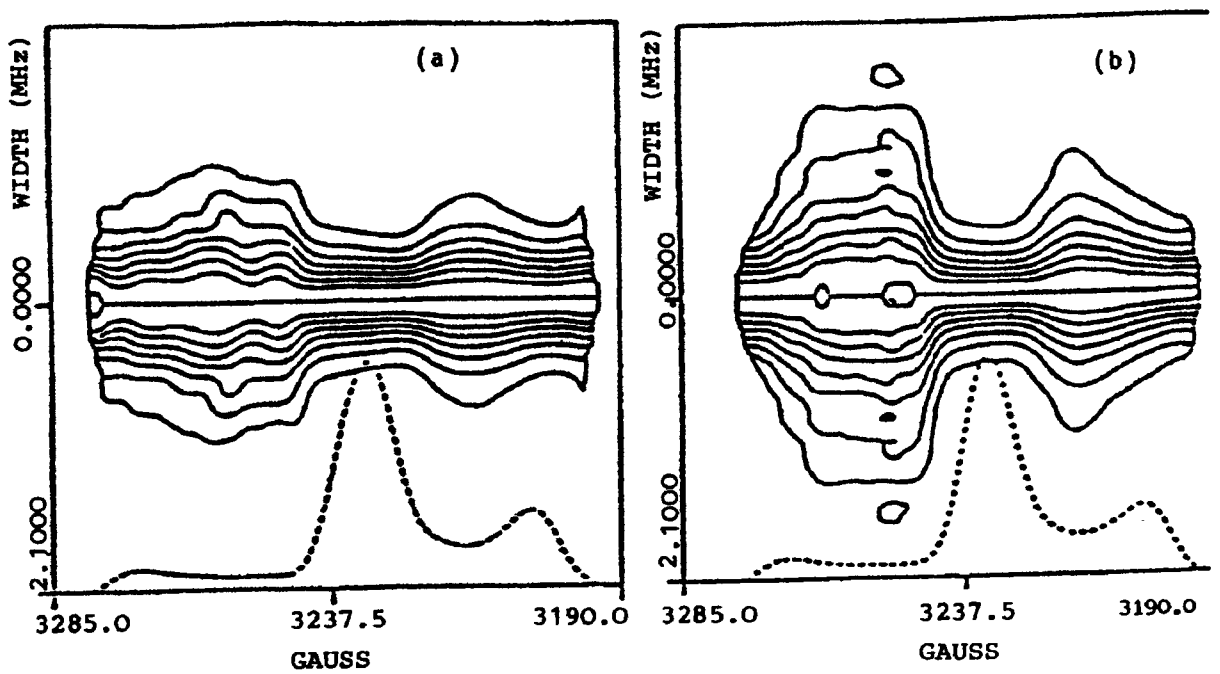

Fig. 22: Normalized contours from spectra of two different nitroxides. (a) shows the spectrum of Tempone in 85% glycerol/H_2O at -75°C. (b) shows the spectrum of CSL in n-butylbenzene at -135°C. The T_M's for these spectra, under these conditions, are approximately the same. (This result was obtained by G.L. Millhauser in these laboratories.)

Two difficulties arise from this approach. First, to avoid so-called FFT window effects, it is necessary to collect data over a considerable time range. This means that a considerable amount of time is spent collecting data when the signal-to-noise ratio is low, and, hence, the spectral resolution is low. This effect is more pronounced in curves with rapidly relaxing components, and so, the resulting distortions are not uniform across the spectrum. The second difficulty arises from the spectrometer dead time, which tends to filter out the more rapidly relaxing components.

To remedy these problems we have found that a linear prediction method (LPSVD [77,78]) for processing the data is very useful for these two dimensional spectra [79] (cf. Fig. 26).

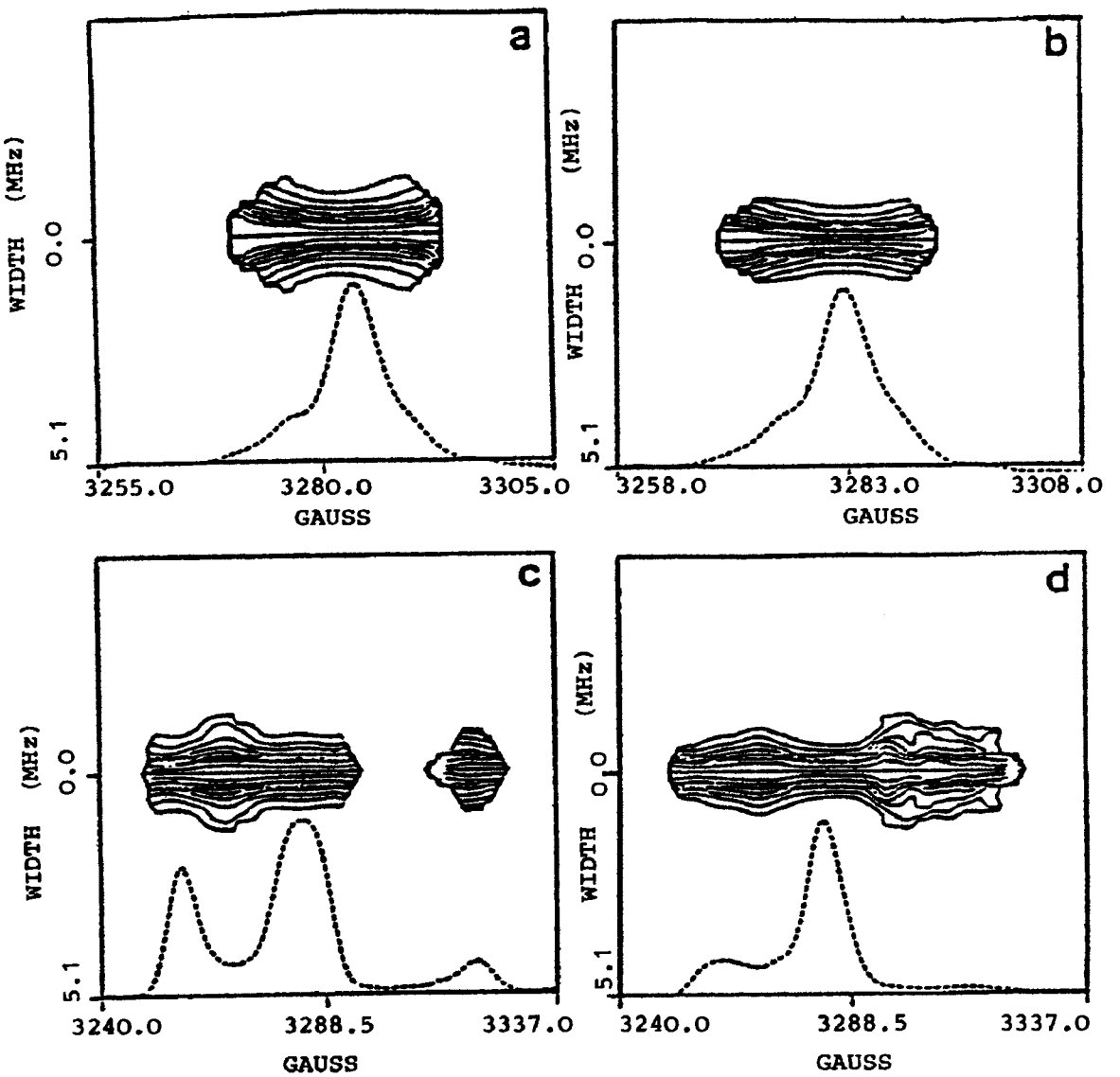

Fig. 23: Normalized contours of experimental spectra from oriented multilayers of low water content DPPC doped with CSL spin probe.

(a) $\theta = 0^{o}$, $T = 0^{o}C$; (b) $\theta = 0^{o}$, $T = -20^{o}C$; (c) $\theta = 90^{o}$, $T = -20^{o}C$;

(d) $\theta = 45^{o}$, $T = -20^{o}C$. (From Ref. [76b].)

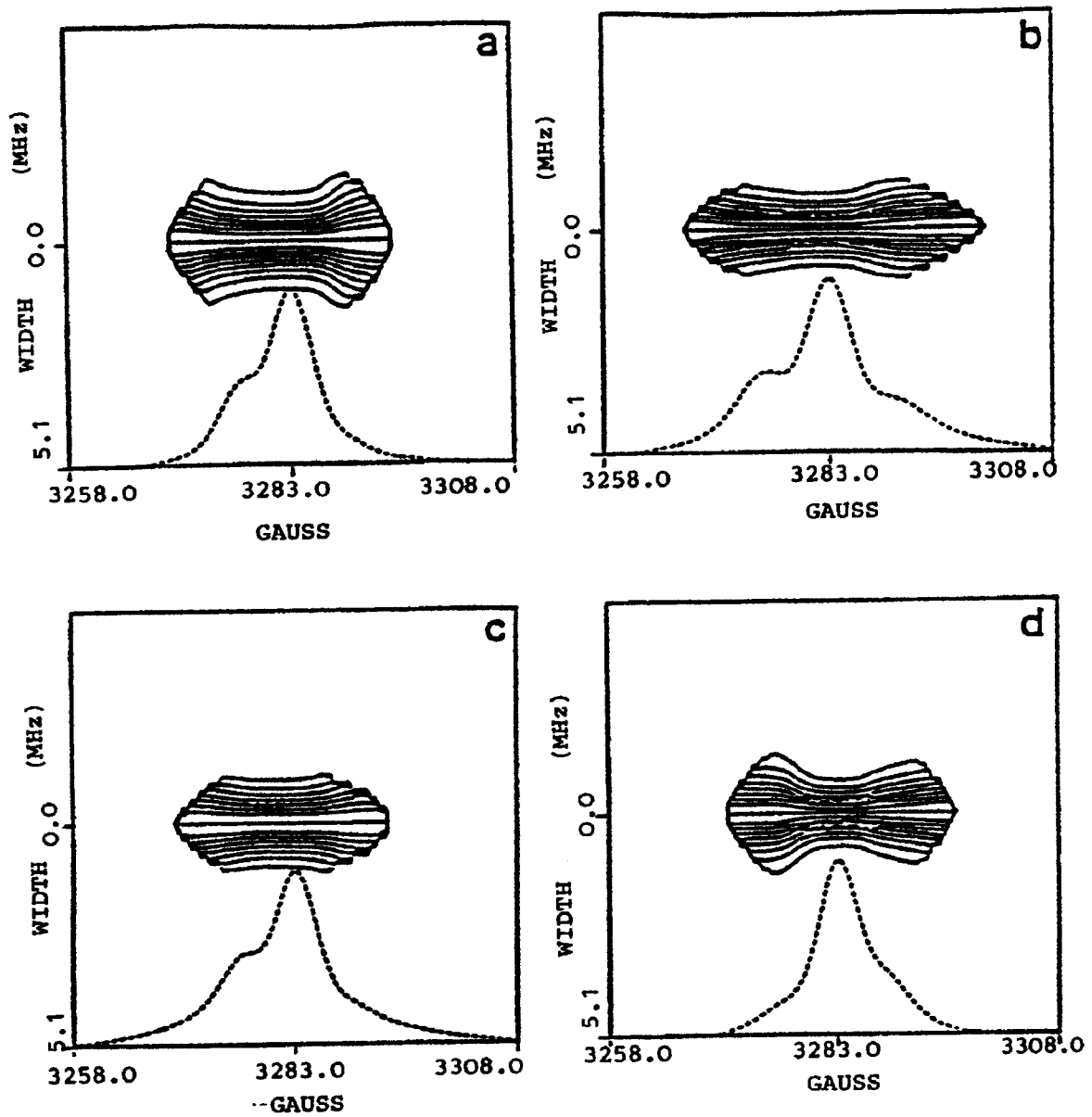

Fig. 24: Normalized contours of simulated DPPC/CSL oriented spectra ($\theta = 0^{o}$) to illustrate the sensitivity to motion and ordering. (a) $R_{||} = 4 \times 10^{4}\ s^{-1}$, $R_{\perp} = 0.8 \times 10^{4}\ s^{-1}$, or $N = 5$, $\lambda_0^2 = 8.0$; (b) $R_{||} = 2 \times 10^{4}\ s^{-1}$, $R_{\perp} = 0.5 \times 10^{4}\ s^{-1}$, $N = 4$, $\lambda_0^2 = 8.0$; (c) $R_{||} = R_{\perp} = 1 \times 10^{4}\ s^{-1}$, $\lambda_0^2 = 4.0$; (d) $R_{||} = R_{\perp} = 1 \times 10^{4}\ s^{-1}$, $\lambda_0^2 = 12.0$. The effects of an intrinsic T_2^{ss} (0.7 μs) due to "solid-state" contributions and inhomogeneous broadening (3.2 gauss) have been included. (From Ref. [76b].)

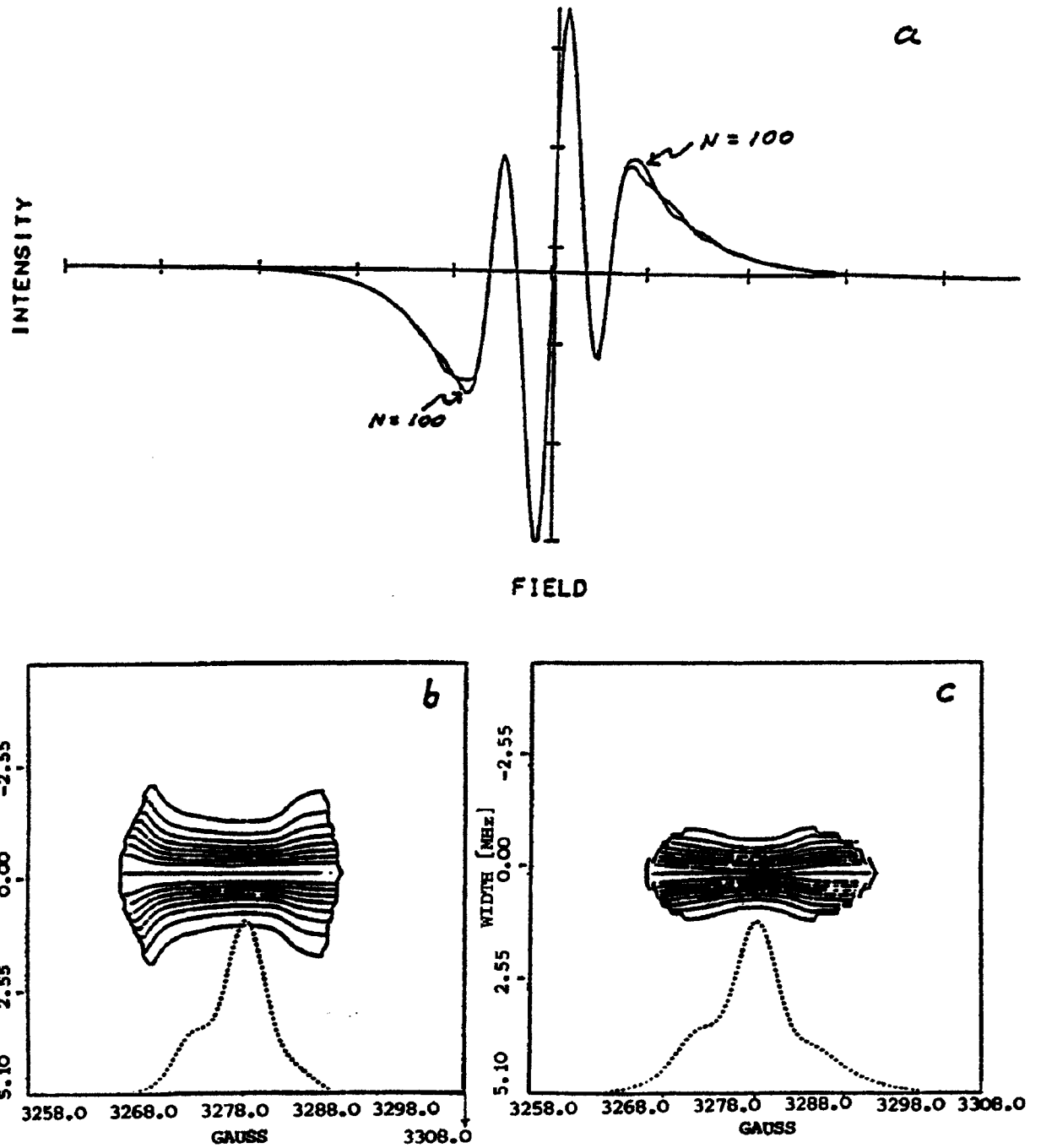

Fig. 25: A comparison of the relative sensitivity of cw vs. 2D ESE to motional anisotropy. (a) Two superimposed spectral simulations where one spectrum has $R_\perp = 10^4\ s^{-1}$ and N = 1, and the other has the same $R_\perp$ but with N = 100. The markers on the x-axis are 9.77 Gauss apart. The normalized contours are simulated from the same parameters with (b) N = 100 and (c) N = 1. Case of high ordering, S = 0.87 and $\theta = 0^0$.

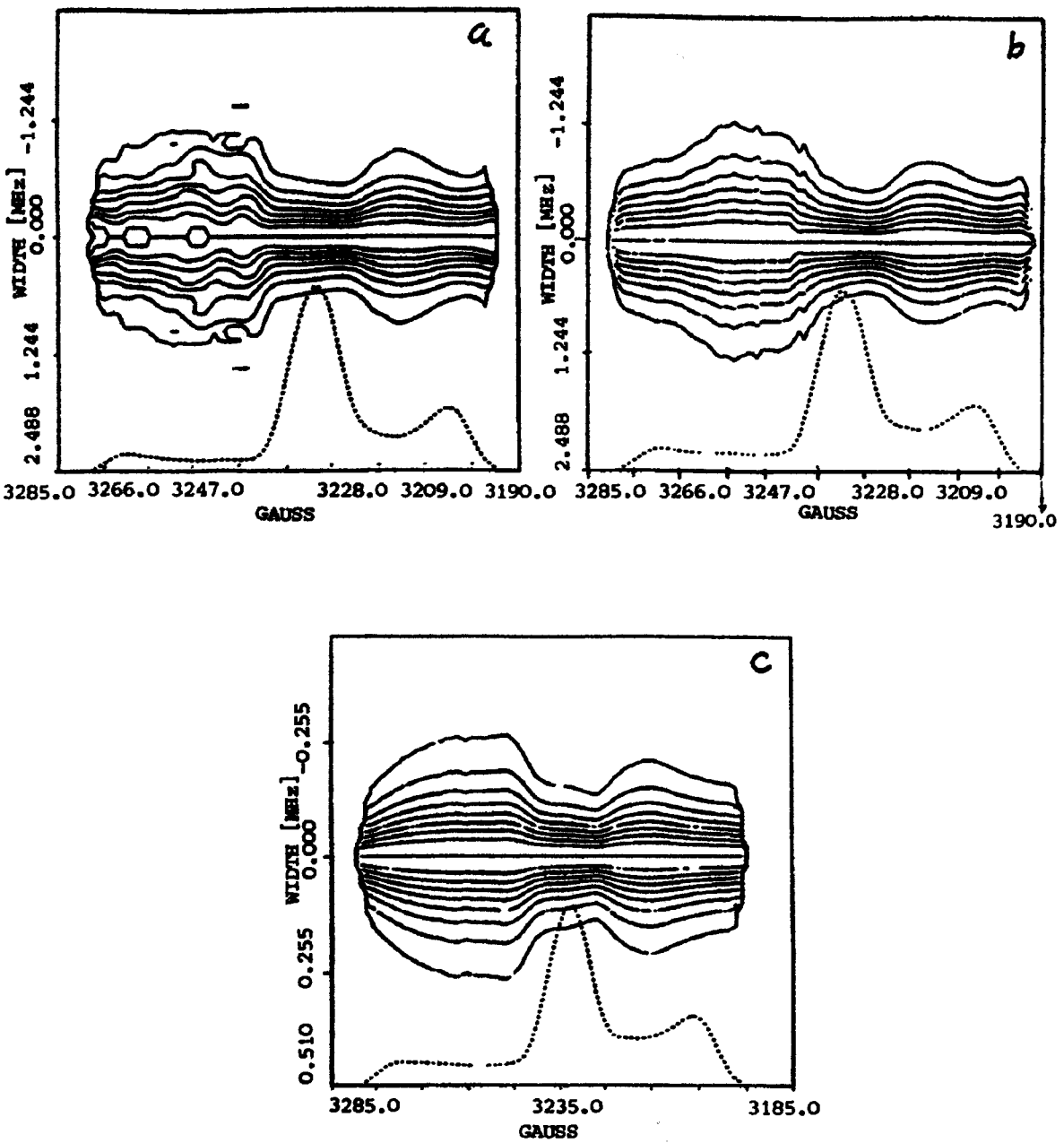

Fig. 26: Normalized contours showing the resolution enhancement obtained from the LPSVD treatment. (a) is from data of Tempone in 85% glycerol/H_2O at -75°C treated by conventional FFT. (b) is from the same data set, but treated with LPSVD. (c) is a different data set that was collected from the same system in a manner that maximizes the efficiency of the LPSVD algorithm. (From Ref. [79].)

C. Newer Techniques

The 2D ESE technique has now been applied to give a map of the rate of magnetization transfer out of each spectral position [80,81]. It is produced by analogy to the "T_2 maps" described above, but is based on the stimulated echo, and it requires one to subtract out the simple T_1 decay. It can produce dramatic indication of the motional model without even requiring sophisticated analysis. We illustrate this in Fig. 27 for the case of physisorbed NO_2 (on a crushed vycor surface), since it dramatically demonstrates anisotropic reorientation (about an axis parallel to the line through the two oxygen atoms labelled as the y-axis. (The study of slow motions on surfaces by a variety of these new methods has recently been reviewed [82].)

Most recently Fourier-Transform (FT) ESR techniques have been developed [71-73], which hold the promise of revolutionizing the use of ESR to study motional dynamics [72,82]. It should permit one-to-two orders of magnitude reduction in experimental times for the 2D-ESE techniques described above, as well as new magnetization transer experiments, in which one could directly correlate the transition rate from one molecular orientation to another by an FT-2D exchange-transfer technique [72].

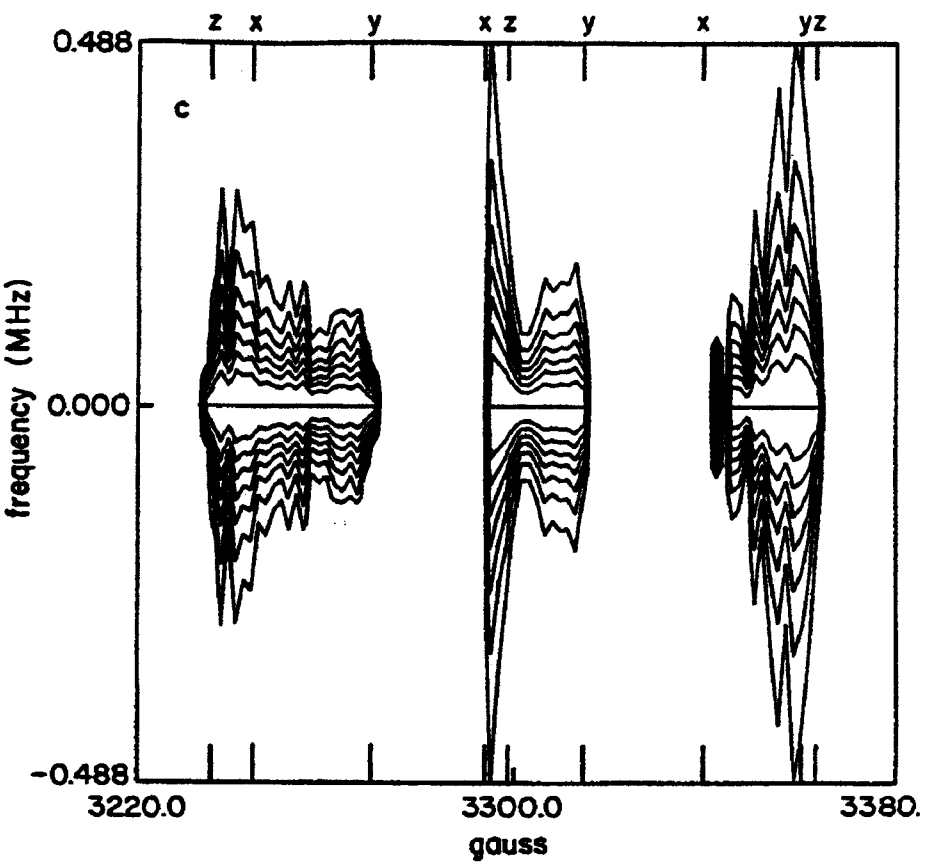

Fig. 27: 2D-ESE contours from the Stimulated Echo sequence for NO_2/Vycor at 35°K showing rates of magnetization transfer. The exponential decay term in T_1 has been subtracted out (from Ref. [80]).

References

[1] L.T. Muus and P.W. Atkins, Eds., Electron-Spin Relaxation in Liquids, Plenum, NY (1972)

[2] L.J. Berliner, Ed., Spin Labeling: Theory and Applications, Academic NY (1976)

[3] M. Dorio and J.H. Freed, Eds., Multiple Electron Resonance Spectroscopy, Plenum, NY (1979)

[4] L. Kevan and R.N. Schwartz, Eds., Time Domain Electron-Spin Resonance, Wiley, NY (1979)

[5] S.A. Zager and J.H. Freed, J. Chem. Phys. 77, 3360 (1982)

[6] D. Kivelson and P.A. Madden, Ann. Rev. Phys. Chem. 31, 523 (1980)

[7] J.L. Dote, D. Kivelson, and R.N. Schwartz, J. Phys. Chem. 85, 2169 (1981)

[8] W.A. Steele, Adv. Chem. Phys. 34, 1 (1976)

[9] G.R. Alms, D.R. Bauer, J.I. Brauman, and R. Pecora, J. Chem. Phys. 58, 5570 (1973); 59, 5310 (1973)

[10] D. Kivelson, M.G. Kivelson, and I. Oppenheim, J. Chem. Phys. 52, 1810 (1970); D. Kivelson, Chem. Soc. Faraday Symp. 11, 7 (1977)

[11] J.S. Hwang, D. Kivelson, and W.Z. Plachy, J. Chem. Phys. 58, 1753 (1973)

[12] D.J. Wilbur and J. Jonas, J. Chem. Phys. 62, 2800 (1975); M. Fury and J. Jonas, ibid. 65, 2206 (1976)

[13] S.A. Zager and J.H. Freed, J. Chem. Phys. 77, 3344 (1982)

[14] J.S. Hwang, R.P. Mason, L.P. Hwang, and J.H. Freed, J. Phys. Chem. 79, 489 (1975)

[15] S.A. Goldman, G.V. Bruno, C.F. Polnaszek, and J.H. Freed, J. Chem. Phys. 56, 712 (1972); 59, 3071 (1973); G.V. Bruno, Ph.D. Thesis, Cornell University (1972)

[16] M. Patron, D. Kivelson, and R.N. Schwartz, J. Phys. Chem. 86, 518 (1982)

[17] B. Blicharska, H.G. Hertz, and H. Versmold, J. Mag. Res. 33, 531 (1980)

[18] C.F. Polnaszek and J.H. Freed, J. Phys. Chem. 79, 2283 (1975)

[19] E. van der Drift and J. Smidt, J. Phys. Chem. 88, 2275 (1984)

[20] R. Wilson and D. Kivelson, J. Chem. Phys. 44, 154 (1966); B. Kowert and D. Kivelson, ibid. 64, 5206 (1976)

[21] J.H. Freed in Ref. [2], Ch. 3.

[22] R.F. Campbell and J.H. Freed, J. Phys. Chem. 84, 2668 (1980)

[23] J.S. Hwang, K.V.S. Rao, and J.H. Freed, J. Phys. Chem. 80, 1490 (1976)

[24] W.J. Lin and J.H. Freed, J. Phys. Chem. 83, 379 (1979)

[25] E. Meirovitch, D. Igner, E. Igner, G. Moro, and J.H. Freed, J. Chem. Phys. 75 3157 (1982)

[26] J.H. Freed, G.V. Bruno, and C.F. Polnaszek, J. Phys. Chem. 75, 3385 (1971)

[27] J.H. Freed, Ann. Rev. Phys. Chem. 23, 265 (1972)

[28] C.F. Polnaszek, G.V. Bruno, and J.H. Freed, J. Chem. Phys. 58, 3185 (1973)

[29] E. Meirovitch and J.H. Freed, J. Phys. Chem. 88, 4995 (1984)

[30] J.H. Freed, J. Chem. Phys. 66, 4183 (1977)

[31] S.A. Zager and J.H. Freed, Chem. Phys. Letts. 109, 270 (1984)

[32] G.J. Krüger, Phys. Rep. 82, 230 (1982)

[33] M.E. Moseley and A. Loewenstein, Mol. Cryst. Liq. Cryst. 90, 117 (1982); 95, 51 (1983)

[34] L.S. Selwyn, R.L. Vold, R.R. Vold, J. Chem. Phys. 80, 5418 (1984)

[35] G. Moro and P.L. Nordio, J. Phys. Chem. 89, 997 (1985)

[36] W.L. McMillan, Phys. Rev. A4, 1238 (1971); 6, 936 (1972)

[37] G. Moro and J.H. Freed, J. Chem. Phys. 74, 3757 (1981)

[38] G. Moro and J.H. Freed, in Large-Scale Eigenvalue Problems, Eds. J. Cullum and R. Willoughby, Vol. 127, Mathematics Studies Series (North-Holland, 1986), 143-160.

[39] G. Moro and J.H. Freed, J. Phys. Chem. 84, 2837 (1980)

[40] G. Moro and J.H. Freed, J. Chem. Phys. 75, 3175 (1981)

[41] G.H. Golub and C.F. Van Loan, Matrix Computations, The John Hopkins University Press, Baltimore, Maryland (1983)

[42] J.K. Cullum and R.A. Willoughby, Lanczos-Algorithms for Large Symmetric Eigenvalue Computations, Vol. I. Birkhauser (Boston, 1985)

[43] K.V. Vasavada, D.J. Schneider, and J.H. Freed, J. Chem. Phys. 86, 647 (1987).

[44] R.G. Gordon and T. Messenger in Ref. [2], Ch. XIII.

[45] A.E. Stillman and J.H. Freed, J. Chem. Phys. 72, 550 (1980)

[46] J.H. Freed in Stochastic Processes - Formalism and Applications, G.S. Agarwal Ed., Lecture Notes in Physics 184, 120 (Springer-Verlag, 1983)

[47] G.P. Zientara and J.H. Freed, J. Chem. Phys. 79, 3077 (1983)

[48] G.P. Zientara and J.H. Freed, Proceedings of the Ninth International Liq. Crystal Conference, Bangalore (1982); G.P. Zientara and J.H. Freed (in preparation)

[49] W.F. van Gunsteren and J.J.C. Berendsen, Mol. Phys. 34, 1311 (1977); P. Rychaert, G. Ciccotti, and J.H.C. Berendsen, J. Comp. Phys. 23, 327 (1977)

[50] G. Zannoni and M. Guerra, Mol. Phys. 44, 849 (1981)

[51] J.F.J. Ypma and G. Vertogen, J. Phys. 37, 557 (1976); Solid State Commun. 18. 475 (1976)

[52] A. Nayeem, Ph.D. Thesis, Cornell University (Oct. 1985)

[53] J.H. Freed (in preparation)

[54] A. Nayeem, V.S.S. Sastry, R. Shankar, and J.H. Freed (in preparation)

[55] K.V.S. Rao, J.S. Hwang, and J.H. Freed, Phys. Rev. Letts. 37, 515 (1976)

[56] a) R.J. Birgeneau, C.w. Garland, G.V. Kasting, and M. Ocko, Phys. Rev. A24, 2624 (1981)
b) C.W. Garland et al., Phys. Rev. A27, 3234 (1983)

[57] P.G. de Gennes, Solid State Commun. 10, 753 (1972)

[58] F. Brochard, J. Phys. (Paris) 34, 411 (1973)

[59] F. Jähnig and F. Brochard, J. Phys. (Paris) 35, 301 (1974)

[60] A.R. Kortan, H. von Känel, R.J. Birgeneau, and J.D. Litster, J. Physique 45, 529 (1984)

[61] A. Nayeem, S. Rananavare, and J.H. Freed (in preparation)

[62] J.P. Hornak, J. Moscicki, D. Schneider, and J.H. Freed, J. Chem. Phys. 84, 3387 (1986)

[63] H. Tanaka and J.H. Freed, J. Phys. Chem. 88, 6633 (1984)

[64] O.H. Griffith and P. Jost, Ch. 12 and H.M. McConnell, Ch. 13 in Ref. [2].

[65] D. Chapman, J.C. Gomez-Fernandez, F.M. Goni, FEBS Lett. 98, 211 (1979) and references therein.

[66] H. Tanaka and J.H. Freed, J. Phys. Chem. 89, 350 (1985)

[67] F. Jähnig, Mol. Cryst. Liq. Cryst. 61, 157 (1981)

[68] W.B. Mims and J. Peisach in Biological Magnetic Resonance, Vol. 3, Eds. L.J. Berliner and J. Reuben, Plenum, NY (1981), Ch. 5 and references therein

[69] J.F. Norris, M.D. Thurnauer, and M.K. Bowman, Adv. Biol. Med. Phys. 17, 365 (1980)

[70] A.E. Stillman and R.N. Schwartz, J. Phys. Chem. 85, 3031 (1981), and references therein

[71] J.P. Hornak and J.H. Freed, J. Mag. Res. 67, 501 (1986)

[72] J. Gorcester and J.H. Freed, J. Chem. Phys. 85, 5375 (1986).

[73] M. Bowman, Bull. Am. Phys. Soc. 31, 524 (1986)

[74] A.E. Stillman, L.J. Schwartz, and J.H. Freed, J. Chem. Phys. 73, 3502 (1980); 76, 5658 (1982)

[75] L.J. Schwartz, A.E. Stillman, and J.H. Freed, J. Chem. Phys. 77, 5410 (1982)

[76] a) G.L. Millhauser and J.H. Freed, J. Chem. Phys. 81, 37 (1984)

b) L. Kar, G.L. Millhauser and J.H. Freed, J. Phys. Chem. 88, 3951 (1984)

[77] R. Kumaresan and D.W. Tufts, IEEE Trans. ASSP-30 833 (1982)

[78] H. Barkhuijsen, R. de Beer, W.M.M.J. Bovée and D. van Ormondt, J. Mag. Res. 61, 465 (1985); D. van Ormondt (private communication).

[79] G.L. Millhauser and J.H. Freed, J. Chem. Phys. 85, 63 (1986)

[80] L.J. Schwartz, G.L. Millhauser and J.H. Freed, Chem. Phys. Letts. 127, 60 (1986)

[81] G.L. Millhauser, Ph.D. Thesis, Cornell University (1986)

[82] G.L. Millhauser, J. Gorcester, and J.H. Freed in Electron Magnetic Resonance of the Solid State, J.A. Weil, Ed. (Can. Chem. Soc. Publication, in press).

[83] D.J. Schneider and J.H. Freed in Lasers, Molecules, Methods, J. Hirschfelder, R. Wyatt, R. Coalson, Eds. (Adv. Chem. Phys., Wiley NY, in press).